Journal of Volcanology and Geothermal Research 373 (2019) 133–147

Contents lists available at ScienceDirect

Journal of Volcanology and Geothermal Research

journal homepage: www.elsevier.com/locate/jvolgeores

Episodes of dormancy and eruption of the Late Pleistocene Ciomadul volcanic complex (Eastern Carpathians, Romania) constrained by zircon geochronology

Kata Molnár [a,b,*], Réka Lukács [c], István Dunkl [d], Axel K. Schmitt [e], Balázs Kiss [c,f], Ioan Seghedi [g], János Szepesi [b,c], Szabolcs Harangi [a,c]

[a] Department of Petrology and Geochemistry, Eötvös Loránd University, Pázmány Péter stny. 1/c, H-1117 Budapest, Hungary
[b] Isotope Climatology and Environmental Research Centre, Institute for Nuclear Research, Hungarian Academy of Sciences, Bem tér 18/c, H-4026 Debrecen, Hungary
[c] MTA-ELTE Volcanology Research Group, Pázmány Péter stny. 1/c, H-1117 Budapest, Hungary
[d] Sedimentology and Environmental Geology, Geoscience Centre, Georg-August Universität Göttingen, Goldschmidtstr. 3, D-37077 Göttingen, Germany
[e] Institute of Earth Sciences, Universität Heidelberg, Im Neuenheimer Feld 234–236, D-69120 Heidelberg, Germany
[f] Institute of Geography and Earth Sciences, Eötvös Loránd University, Pázmány Péter stny. 1/c, H-1117 Budapest, Hungary
[g] Institute of Geodynamics, Romanian Academy, 19–21 Jean-Louis Calderon St., R-020032 Bucharest-37, Romania

ARTICLE INFO

Article history:
Received 26 October 2018
Received in revised form 18 January 2019
Accepted 31 January 2019
Available online 08 February 2019

Keywords:
Combined zircon U-Th and (U-Th)/He dating
Repose time
Magma output rate
Monotonous geochemistry
Eruption chronology
Eastern Carpathians

ABSTRACT

Ciomadul is the youngest volcanic system in the Carpathian-Pannonian Region recording eruptive activity from ca. 1 Ma to 30 ka. Based on combined zircon U-Th and (U-Th)/He geochronology, Ciomadul volcanism is divided into two main eruptive periods: Old Ciomadul (1 Ma – 300 ka; OCEP) and Young Ciomadul Eruptive Period (160–30 ka; YCEP). OCEP activity comprises Eruptive Epochs 1–3, whereas new ages for eight lava domes and four pyroclastic units belonging to the YCEP lead to its further subdivision into two eruptive epochs: Eruptive Epochs 4 and 5. The extrusion of most of the lava domes occurred between 160 and 90 ka (Eruptive Epoch 4) during three eruptive episodes at ca. 155 ka, 135 ka and 95 ka (Eruptive Episodes 4/1, 4/2 and 4/3, respectively) along a NE-SW lineament, which is perpendicular to the regional NW-SE trend of the Călimani-Gurghiu-Harghita volcanic chain. Eruptive Epoch 5 occurred after a ca. 40 kyr of quiescence at ca. 55–30 ka, and is mainly characterized by explosive eruptions with a minor lava dome building activity. All of the dated pyroclastic outcrops, together with the lava dome of Piscul Pietros, belong to the older Eruptive Episode 5/1, with an eruption age of 55–45 ka. The eruption centers of Eruptive Epoch 5 are located at the junction of the conjugated NW-SE and NE-SW lineaments defined by the older eruptive centers. The whole-rock geochemistry of all studied samples is fairly homogeneous (SiO_2 = 63–69 wt%, K_2O = 3–4 wt%). It also overlaps with the composition of the lava domes of the Old Ciomadul Eruptive Period, implying a monotonous geochemical characteristic for the past 1 Myr. The eruption rates for the Ciomadul volcanism were determined based on the erupted lava dome volume calculations, supplemented with the eruption ages. The activity peaked during the Eruptive Epoch 4 (160–90 ka), having an eruption rate of 0.1 km^3/kyr. In comparison, these values are 0.05 km^3/kyr for the YCEP (160–30 ka) and 0.01 km^3/kyr for the overall Ciomadul volcanism (1 Ma–30 ka). Based on the geochemical characteristics, the quiescence periods and the lifetime of the complex, as well as the relatively small amount of erupted material, this volcanic system can be placed in a subduction-related post-collisional geodynamic setting, which shows strong chemical similarities to continental arc volcanism. The commonly found long repose times between the active phases suggest that the nature of a volcano cannot be understood solely based on the elapsed time since the last eruption. Instead, comprehensive geochronology, coupled with the understanding of the magma storage behavior could be a base of hazard assessment for volcanic fields, where the last eruptions occurred several 10's of thousand years ago and therefore they are not considered as potentially active.

1. Introduction

Understanding the frequency of eruptions in long-lived volcanic complexes is important to evaluate their potential hazards especially when these systems remained dormant for protracted periods. Many

* Corresponding author at: Department of Petrology and Geochemistry, Eötvös Loránd University, Pázmány Péter stny. 1/c, H-1117 Budapest, Hungary.
E-mail address: molnar.kata@atomki.mta.hu (K. Molnár).

https://doi.org/10.1016/j.jvolgeores.2019.01.025
0377-0273/

intermediate (andesitic-dacitic) volcanic systems in continental arc or collision zones are characterized by long (>100 kyr) dormancy periods after which volcanism is rejuvenated (Hildreth and Lanphere, 1994; Hoshizumi et al., 1999; Gamble et al., 2003; Hora et al., 2007; Bablon et al., 2018; Molnár et al., 2018), often with explosive eruptions (Frey et al., 2014). Thus, protracted quiescence since the last volcanic eruption may be misleading in estimating eruptive recurrence and the potential for volcanic reawakening. In fact, there are many long-dormant volcanoes world-wide which erupted several 10s of thousand years ago, but melt-bearing magma still can be detected beneath them and therefore, renewal of volcanism cannot be excluded (e.g., Colli Albani, Italy, last erupted ca. 36 ka; Freda et al., 2006; Trasatti et al., 2018). Since the potential of reawakening is controlled mostly by the state of the subvolcanic magma storage, Harangi et al. (2015a, 2015b) suggested the acronym PAMS (Potentially Active Magma Storage) for such long-dormant volcanoes where melt presence is either evident from geophysical observation, or from extrapolation of geochemical indicators such as protracted zircon crystallization in older eruptions. A detailed eruptive chronology of such volcanic systems combined with calculations of erupted volumes can help to better constrain eruptive recurrence over long time intervals, which is fundamental for hazard assessment.

Ciomadul is a volcanic complex in eastern-central Europe where the last known eruption occurred at around 30 ka (e.g., Vinkler et al., 2007; Harangi et al., 2010, 2015a; Karátson et al., 2016). However, its earlier eruption history shows prolonged, often extending over >100 kyr quiescence periods between eruptions (Molnár et al., 2018). Combined zircon U-Th-Pb and (U-Th)/He dating (e.g., Schmitt et al., 2006, 2010; Danišík et al., 2012, 2017) proved to be particularly suitable in dating rocks from these Quaternary (<1 Ma) eruption events where other geochronologically suitable mineral phases such as K-feldspar are lacking. The combined zircon U-Th-Pb and (U-Th)/He ages (Harangi et al., 2015a; Molnár et al., 2018) considerably refined the eruption chronology of Ciomadul, which was previously based mainly on K/Ar geochronology (Pécskay et al., 1995, 2006; Szakács et al., 2015). Molnár et al. (2018) summarized results for age determinations of the earlier lava dome building stage between ca. 1 Ma and 300 ka, whereas Harangi et al. (2015a) characterized the youngest eruption stage from 56 ka to 32 ka. Here, we complete this data set with new results on the lava dome extrusion period of Ciomadul and its bulk rock geochemistry. Summarizing these results, we develop a conceptual model for the volcanism of this long-dormant volcanic system using the volcanic activity unit-based methodology of Fisher and Schmincke (1984) and Lucchi (2013). Based on these new eruption ages, we also refine the eruption rate calculations presented by Szakács et al. (2015).

2. Geological and volcanological background

Ciomadul is the youngest manifestation of the Neogene-Quaternary volcanism of the Carpathian-Pannonian Region which evolved over the past ca. 20 Ma (Fig. 1; Szabó et al., 1992; Seghedi et al., 1998, 2004, 2005; Harangi, 2001; Konečný et al., 2002; Harangi and Lenkey, 2007; Lexa et al., 2010; Seghedi and Downes, 2011; Lukács et al., 2018a). It consists of a volcanic dome field with a massive central volcanic complex. The scattered lava domes with dacitic, andesitic and shoshonitic composition formed episodically between ca. 1 Ma and 300 ka with eruptive pulses separated by long (>100 kyr) quiescent periods ("Old Ciomadul" eruption stage; Molnár et al., 2018). The Ciomadul volcanic complex is by far the most voluminous volcanic product within this volcanic field (Szakács et al., 2015), and it developed within the last 200 kyr ("Young Ciomadul" eruption stage; Moriya et al., 1995, 1996; Vinkler et al., 2007; Harangi et al., 2010, 2015a; Karátson et al., 2013, 2016). The Ciomadul volcanic dome field is located at the southeastern edge of the Călimani-Gurghiu-Harghita andesitic-dacitic volcanic chain (Fig. 1) which extends over ~160 km and is characterized by a gradual shift of the eruption center location towards southeast coupled with a gradual decrease in eruptive volumes (Fig. 1; Pécskay et al., 1995; Szakács and Seghedi, 1995; Mason et al., 1996; Karátson and Tímár, 2005). The location of Ciomadul at the end of this chain causes it to pierce and overlay flysch deposits of the Carpathian collisional zone and rocks of the Cretaceous Ceahlau-Severin nappe at the southern margin of the Plio-Pleistocene intramontaneous Ciuc-basin (Szakács et al., 1993; Figs. 1, 2).

Volcanic activity in the South Harghita (Luci-Lazu, Cucu, Pilişca and Ciomadul) started at 5.3 Ma (Pécskay et al., 1995), whereas the youngest activity is represented by explosive eruptions of the Ciomadul volcanic complex at ca. 30 ka (Vinkler et al., 2007; Harangi et al., 2010, 2015a; Karátson et al., 2016). Two sharp compositional changes in the erupted magmas occurred during the 3.9–2.8 Ma and 1.6–1.0 Ma gaps (Pécskay et al., 2006; Seghedi et al., 2011; Molnár et al., 2018). After

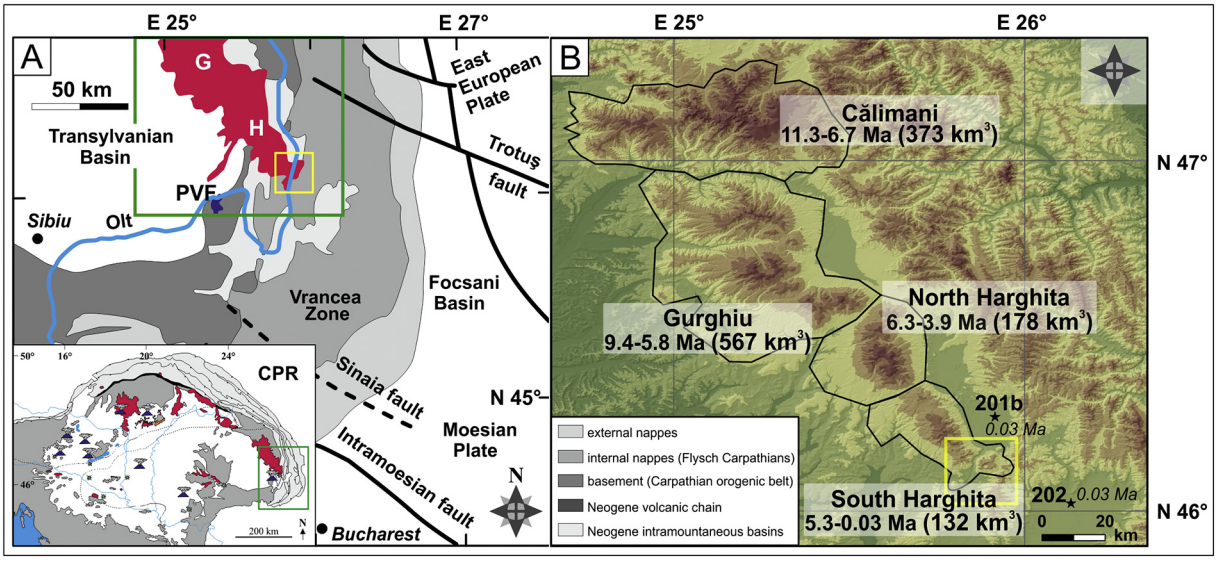

Fig. 1. Simplified tectonic (A) and geographic/relief (B) map of the Călimani-Gurghiu-Harghita volcanic chain with the previously reported age intervals and overall erupted magma volumes (after Szakács and Seghedi, 1995; Pécskay et al., 1995, 2006; Karátson and Tímár, 2005; Martin et al., 2006; Karátson, 2007 and Vinkler et al., 2007). G: Gurghiu; H: Harghita; PVF: Perşani Volcanic Field. Green and yellow rectangles refer to Figs. 1B and 2, respectively. Eruption ages of the two distal pyroclastic deposits (201b and 202; Harangi et al., 2015a, 2018) are indicated in italic. (For interpretation of the references to color in this figure legend, the reader is referred to the web version of this article.)

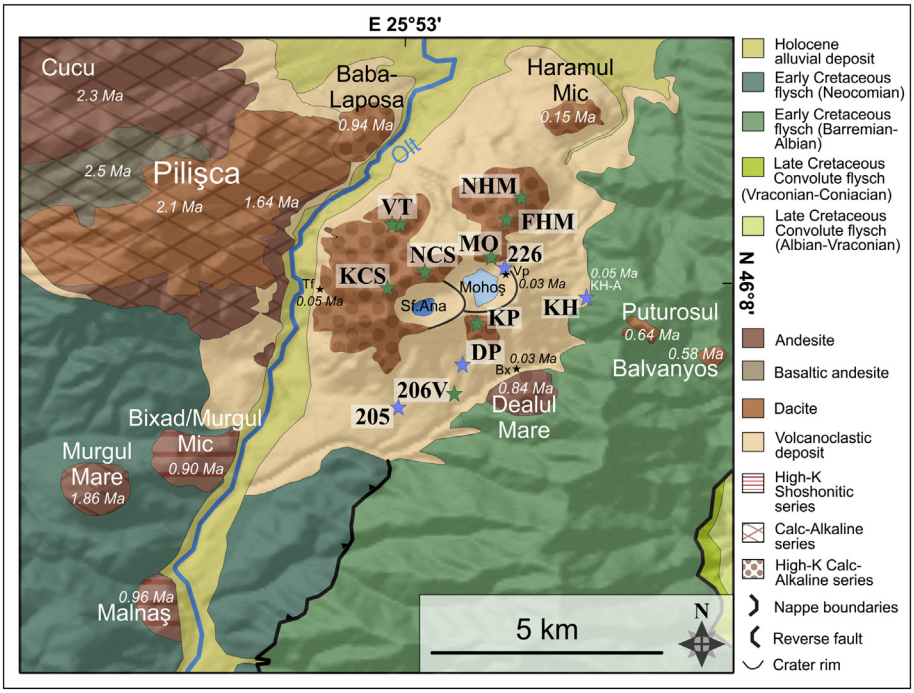

Fig. 2. Geological map of the South Harghita with the sampling sites (modified after Seghedi et al., 1987; Molnár et al., 2018). Blue and green stars refer to pyroclastic deposits and lava dome samples, respectively, for their sample names and localities please refer to Table 1. Eruption ages of the previously dated lava domes (Szakács et al., 1993, 2015; Pécskay et al., 1995; Molnár et al., 2018) and pyroclastic outcrops (as KH-A: MK-4, Tf: MK-3, Vp: MK-1, Bx: MK-5 in Harangi et al., 2015a; black stars) are indicated in italic. (For interpretation of the references to color in this figure legend, the reader is referred to the web version of this article.)

the first hiatus, eruptive rocks became more potassic and enriched in incompatible elements compared to the earlier volcanism (Mason et al., 1996; Harangi and Lenkey, 2007; Seghedi et al., 2011), whereas magmas erupted after the second (1.6–1.0 Ma) gap became more enrichment in K, Ba and Sr but depleted in heavy rare earth elements (Seghedi et al., 1987; Vinkler et al., 2007; Molnár et al., 2018).

Ciomadul is situated within a geodynamically active setting ~60 km northwest of the Vrancea zone (Fig. 1) where frequent earthquakes with deep hypocenters indicate a descending, near-vertical, dense and cold lithospheric slab into the upper mantle (Oncescu et al., 1984; Sperner et al., 2001; Martin et al., 2006; Fillerup et al., 2010). Moreover, the monogenetic alkaline basaltic Perşani Volcanic Field which formed more or less contemporaneously (1.2–0.6 Ma; Panaiotu et al., 2013) with the "Old Ciomadul" eruptive stage (1.0–0.3 Ma; Molnár et al., 2018) is located ~40 km west of Ciomadul (Fig. 1). The relationship between the slab descending beneath Vrancea and the formation of the two compositionally contrasting volcanic fields remains debated (e.g., Gîrbacea and Frisch, 1998; Sperner et al., 2001; Fillerup et al., 2010; Seghedi et al., 2011).

The Ciomadul volcanic complex comprises amalgamated dacitic lava domes truncated by two deep explosion craters (Mohoş and Sf. Ana; e.g. Szakács and Seghedi, 1995; Szakács et al., 2015; Karátson et al., 2013, 2016). It is the youngest manifestation of volcanism within the Ciomadul volcanic dome field. A tightly-spaced dome complex dominates the western and northern walls of the craters whereas mainly explosive eruptive products crop out on the eastern and southern flanks of the volcano (Fig. 2). The initial lava dome-building stage of the Ciomadul volcanic complex took place at ca. 200–100 ka (Karátson et al., 2013), which was followed by dominantly explosive eruptions (pyroclastic fall and flow deposits of Vulcanian to sub-Plinian eruptions) with minor lava dome extrusions (Harangi et al., 2015a; Karátson et al., 2016). This second stage occurred between 57 and 32 ka based on disequilibrium corrected zircon (U-Th)/He geochronology (Harangi et al., 2015a). Geophysical studies suggest the presence of a melt-bearing magma body beneath the volcano (Popa et al., 2012; Harangi et al., 2015b) which is consistent with a large range of zircon crystallization ages indicative of prolonged magma residence time (Harangi et al., 2015a; Lukács et al., 2019). Kiss et al. (2014) pointed out that the long-lasting felsic crystal mush can be effectively and rapidly reactivated by ascending hot mafic magmas.

3. Samples

3.1. Lava dome samples

The collected fresh dacitic lava dome samples represent most of the volcanic domes bordering the twin-craters of the Ciomadul volcanic complex (Figs. 2, 3, Table 1). Additionally, a remnant of a lava flow at the southern flank of the volcano exposed along the Pârâul Disznyó was also sampled (206 V) together with the younger Piscul Pietros lava dome. The Piscul Pietros dome was already dated in a previous study ("MK-208" in Harangi et al., 2015a) but it was included in this study to refine its extent and age (Fig. 2; Table 1). In case of those locations where preliminary disequilibrium uncorrected (U-Th)/He zircon data were already published (Ciomadul Mic, Haramul Ierbos and Dealul Cetăţii; Karátson et al., 2013), new combined zircon U-Th and (U-Th)/He dating was performed.

3.2. Pyroclastic deposits

We completed the eruption chronology of the explosive volcanism by additional sampling and dating (Figs. 2, 4, Table 1). This dataset is complemented by the eruption ages of two distal deposits, and ages for previously dated proximal deposits (Harangi et al., 2015a).

3.2.1. DP outcrop

A ~25 m long, ~3–5 m height block-and-ash flow and pyroclastic flow deposit is exposed alongside the Pârâul Disznyó, further upstream from the outcrop 206 V, ~ 900 m north of the No. 113 Community Road. The sequence starts with a block-rich debris-flow deposit covered by a poorly sorted, clast-supported, ~3 m thick block-and-ash flow layer, containing black, glassy and grey dacitic juvenile lithoclasts within a

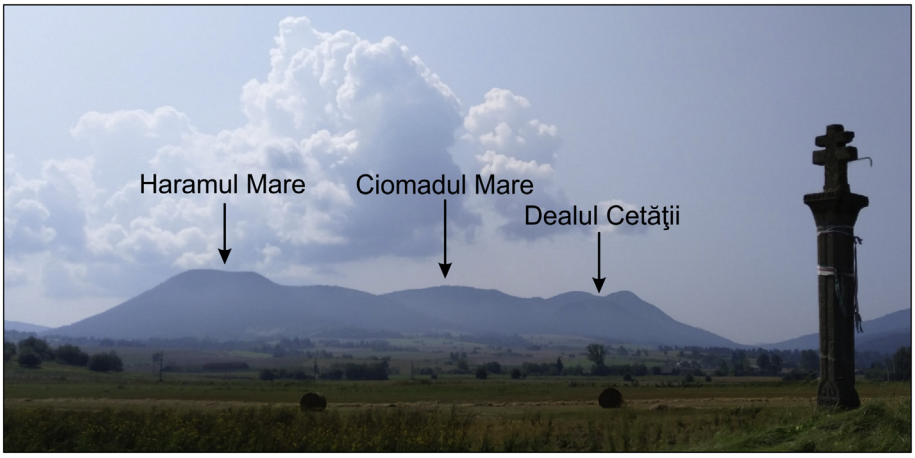

Fig. 3. The Ciomadul volcanic complex from the north with the domes of Haramul Mare, Ciomadul Mare and Dealul Cetăţii.

coarse ash matrix (Fig. 4A). A ~1–2 m thick, matrix-supported pyroclastic flow deposit overlies the block-and-ash flow deposit with an indistinct transition. Pumices were collected from the lower, block-and-ash flow layer.

3.2.2. 205b outcrop

This pyroclastic deposit is located also on the southern flank, described by Karátson et al. (2016) as a block-and-ash flow deposit ("BIX-2"). The outcrop is exposed as >3.5 m thick, coarse-grained, poorly sorted, brecciated unit with occasional prismatic jointed dacitic blocks (Fig. 4B).

3.2.3. KH outcrop

A sequence of pyroclastic flow- and fall-units is exposed in a ~5–7 m deep, ~50 m long gully east of Mohoş crater. The major part of the outcrop is dominated by pyroclastic surges, flows and fall deposits. Its lowermost layer ("BOL-1.0 in Karátson et al., 2016) is a thick, massive, pumiceous lapillistone. This layer was already dated by the combined zircon U-Th and (U-Th)/He method ("KH-A" in this study, Fig. 4C; "MK-4" in Harangi et al., 2015a), and the oldest eruption age of 55.9 (+2.2, −2.3) ka for the last phase of the Ciomadul volcanism was obtained for this sample. Here, the uppermost part (KH-N; identical to the "BOL-1.2" layer in Karátson et al., 2016) of the outcrop was sampled comprising a ~35 cm thick, clast-supported, poorly sorted layer containing large amount (>10%) of dark, glassy dacitic lithoclasts (Fig. 4C). Both layers are interpreted by Karátson et al. (2016) as dense, massive pyroclastic density current deposits although we cannot exclude that they originated as proximal pyroclastic fall out.

3.2.4. 226 outcrop

This outcrop is exposed on the eastern flank of the volcano, situated on the northeastern side of Tinovul Mohoş. At the time of sampling the outcrop was ~3 m high and consisted of four layers of pyroclastic flow and fall deposits (Fig. 4D, E; "MOH-VM-1" in Karátson et al., 2016). Pumices were sampled from the ~40 cm thick, polymictic, grain-supported, moderately sorted lowermost layer (226c; identical to "MOH-VM-1.1 in Karátson et al., 2016) and from the ~70 cm thick, unsorted, pumice-dominated pyroclastic breccia with ~5% dark, glassy dacitic lithoclasts at the top (226-4b; upper part of "MOH-VM-1.3 in Karátson et al., 2016). We correlated the 226c bed with that of KH-A because of similar volcanological features whereas the 226-4b layer is of similar character as the KH-N layer.

Table 1
Sample names, localities, lithology and previous age results for the studied samples of the Ciomadul volcanic complex. The corresponding Hungarian names are indicated in italic. l.r. = lava rock; p. = pumice.

Sample code in the text	Location	Coordinate		type	Previous results		
		N	E		Dated fraction	Age (ka)	Reference
NCS	Ciomadul Mare – *Nagy-Csomád*	46°8′11″	25°53′19″	l.r.	Zircon	150–130[a]	Molnár (2014)
FHM	Haramul Ierbos – *Fűharam*	46°9′2.16″	25°54′38.51″	l.r.	Zircon	140–110[a]	Karátson et al. (2013)
VT	Dealul Cetăţii – *Vártető*	46°8′56.98″	25°52′55.31″	l.r.	Whole rock	400 ± 160[b]	Szakács et al. (2015)
		46°8′57.67″	25°52′47.51″	l.r.		430 ± 109[b]	Szakács et al. (2015)
					Zircon	140–120[a]	Karátson et al. (2013)
KCS	Ciomadul Mic – *Kis-Csomád*	46°7′55″	25°52′43	l.r.	Zircon	140–80[a]	Karátson et al. (2013)
MO	Mohoş – *Mohos*	46°8′22.88″	25°54′23.60″	l.r.	–		
NHM	Haramul Mare – *Nagy-Haram*	46°9′23″	25°54′53″	l.r.	Whole rock	590 ± 200[b]	Pécskay et al. (1995)
					Zircon	90–70[a]	Molnár (2014)
206 V	Pârâul Disznyó – *Disznyó-patak*	46°6′12.92″	25°53′47.67″	l.r.	–		
KP	Piscul Pietros – *Kövesponk*	46°7′14.74″	25°54′12.30″	l.r.	Biotite	290 ± 110[b]	Szakács et al. (2015)
					Zircon	42.9 ± 1.5[c]	Harangi et al. (2015a)
205b	Bixad - *Bükszádi út*	46°5′59.65″	25°52′53.85″	p.	–		
DP	Pârâul Disznyó – *Disznyó-patak*	46°6′41″	25°53′56″	p.	–		
226c	Mohoş – *Mohos-láp kivezető út*	46°8′13.74″	25°54′34.03″	p.	–		
226-4b		46°8′13.74″	25°54′34.03″	p.	–		
KH-N	Câmpul Lung – *Kovászna-Hargita megyehatár*	46°7′46″	25°55′54″	p.	–		
KH-A	Câmpul Lung – *Kovászna-Hargita megyehatár*	46°7′46″	25°55′54″	p.	Zircon	55.9 ± 2.2[c]	Harangi et al. (2015a)

[a] Disequilibrium uncorrected (U-Th)/He ages.
[b] K/Ar ages.
[c] Combined zircon U-Th and (U-Th)/He ages.

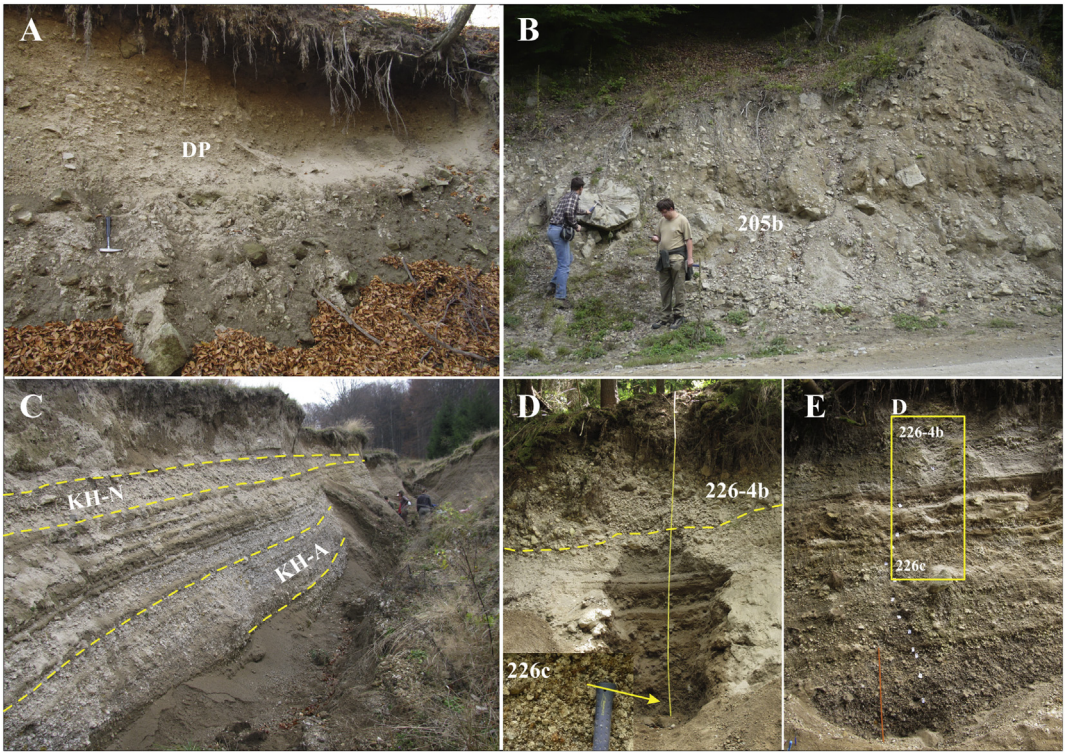

Fig. 4. The sampled pyroclastic outcrops: A – KH, KH-A is the previously sampled and dated layer (as MK-4, 56 ± 2 ka in Harangi et al., 2015a); B, C – 226; D – DP; E – 205b.

4. Analytical methods

4.1. Petrography and whole rock analysis

Polished thin sections were prepared from the dacitic lava dome rocks and pumices for the petrological analysis. A Nikon Eclipse E600 POL type polarization microscope equipped with a Nikon CoolPIX E950 type camera was used for the petrographic descriptions at the Department of Petrology and Geochemistry, Eötvös Loránd University (Budapest, Hungary).

Whole-rock major and trace element geochemical compositions were analyzed at AcmeLabs Ltd. (Vancouver, Canada; http://acmelab.com/). Major and minor elements were determined by ICP-emission spectrometry and trace elements were analyzed by ICP-MS following a lithium borate fusion and dilute acid digestion. The cumulative result of the whole-rock analysis is presented in the Supplementary material.

4.2. Zircon extraction

Approximately 1 kg of rock was collected from each outcrop. Samples were crushed and sieved, and the 63–250 μm fractions were separated in heavy liquid (sodium polytungstate with a density of 2.88 ± 0.01 g/cm^3). Zircon crystals were concentrated by removing Fe-Ti oxides using a Nd-alloy hand magnet. The crystals from the pumices were cleaned by short HF treatment in order to remove the glass from their surface. Fissure-free intact, euhedral zircon crystals of minimum 60 μm width were hand-picked from the non-magnetic fraction under a binocular microscope, photographed and packed into platinum capsules for He degassing. General features, size and shape characteristics of the selected crystals are presented in the Supplementary material.

4.3. U-Th analysis

Zircon crystals were mounted in indium and their U-Th isotopic compositions analyzed using the University of California Los Angeles (USA) and Heidelberg University (Germany) large magnet radius ion microprobes (CAMECA ims 1270 and 1280-HR, respectively). Analytical procedures are described in Schmitt et al. (2006), with the modification of using multi-collector detection (Schmitt et al., 2017). Accuracy of the relative sensitivity calibration for U/Th and background corrections were monitored by replicate analysis of equilibrium zircon standard AS3 mounted next to the unknowns (1099.1 Ma; Paces and Miller Jr., 1993). The average for AS3 analyzed interspersed with the unknowns yielded a secular equilibrium ratio for (^{230}Th)/(^{238}U) deviation from unity within <1%. Uranium concentrations were estimated from $UO^+/Zr_2O_4^+$ intensity ratios relative to zircon standard 91,500 (81.2 ppm U; Wiedenbeck et al., 2004). Crystallization ages were calculated as two-point isochron using zircon and melt with Th/U = 3.58 from Harangi et al. (2015a).

4.4. (U-Th)/He analysis

(U-Th)/He age determinations were carried out at the GÖochron Laboratory of Georg-August University (Göttingen, Germany). Analytical procedures are described in detail in Molnár et al. (2018). The accuracy of zircon (U-Th)/He dating was monitored by replicate analyses of the reference material of Fish Canyon Tuff zircon, yielding a mean (U-Th)/He age of 28.1 ± 2.3 Ma (n = 128; where n is the number of replicate analyses per sample) which consistent with the reference (U-Th)/He age of 28.3 ± 1.3 Ma (Reiners, 2005). The results of the (U-Th)/He ages are presented in the Supplementary material.

The combined zircon U-Th and (U-Th)/He ages were computed using the MCHeCalc software (http://sims.ess.ucla.edu/Research/MCHeCalc.php) following the description provided by Schmitt et al. (2010). Zircon/magma D_{230} parameters (Farley et al., 2002) were calculated using the Th/U ratios of analyzed bulk zircon crystals and whole rock (Supplementary material). Secular equilibrium for ^{231}Pa (i.e. D_{231} = 1) was assumed because the ^{4}He contribution from the ^{235}U decay series is minor, and the effects of disequilibrium are negligible within reasonable limits of D_{231} (Schmitt, 2011). Uncertainties for the average crystallization age corrected samples were calculated by multiplying the 2-sigma error with the square root of the MSWD (e.g., Danišík

et al., 2012; Molnár et al., 2018), and 2-sigma uncertainties are stated for the double-dated samples propagating individual U-Th and (U-Th)/He age uncertainties. In case of double-dating, error-weighted average ages (Schmitt et al., 2014) were calculated (Fig. 8; Suppl. mat.).

4.5. Erupted volume calculations

The dense rock equivalent (DRE) erupted volumes of Ciomadul and the associated lava dome units (Fig. 9) were determined using ArcGIS analytical tools on SRTM global digital elevation models (DEM, https://lta.cr.usgs.gov/SRTM1Arc). The lateral resolution of the DEMs is 1 arc sec (30 m) for global coverage. The digitized margins (Szakács et al., 2015; Molnár et al., 2018) of each volcanic feature were used for DEM segmentation. The boundaries were digitized on Google Earth imagery. The volumes were calculated applying a base level, determined from surrounding topography. All volume calculations are very sensitive to the chosen baseline; thus considering the morphological parameters (height, diameter), the uncertainty of the volumetric calculations is ~20% (Frey et al., 2004).

5. Results

5.1. Petrography and geochemistry

The lava domes are typically crystal-rich (~35–40 vol%), porphyritic rocks with a phenocryst-assemblage of plagioclase, amphibole and biotite. Olivine, clinopyroxene, K-feldspar and quartz occasionally occur. The presence of felsic (plagioclase ± amphibole, biotite) crystal clots is frequent, whereas mafic (amphibole ± clinopyroxene, plagioclase, olivine) crystal clots and individual Mg-rich crystals are only present in few lava dome rocks. The groundmass is totally crystalline and consists of plagioclase microlites and Fe-Ti oxides. The lava dome rocks are rich in accessories such as zircon, apatite and titanite. Pumices are mineralogically very similar to the lava dome rocks at lower levels of crystallinity (25–30 vol% vesicle-free). The phenocrysts in pumice are plagioclase, amphibole and biotite. The vesicular groundmass is composed of glass, plagioclase microlites and rarely Fe-Ti oxides. Both, lava dome and pumice samples display disequilibrium textures implying open-system magma chamber processes involving mixing of distinct magmas as described by Kiss et al. (2014). No relationship was found between the eruption ages and the bulk composition of the erupted magma.

Bulk rock geochemical data for the Ciomadul volcano were reported first by Seghedi et al. (1987) followed by Mason et al. (1996, 1998), Harangi and Lenkey (2007), Vinkler et al. (2007) and Seghedi et al. (2011), whereas composition of the older lava domes in the Ciomadul Volcanic Dome Field was presented by Molnár et al. (2018). This dataset was completed here with the new bulk rock compositional data (Suppl. Mat.).

Lava dome and pumice samples are exclusively high-K calc-alkaline dacites (K_2O = 3–4 wt%; Peccerillo and Taylor, 1976; Fig. 5). Collectively, the form a linear trend ranging from 63 to 69 wt% SiO_2 (Fig. 5). The Ciomadul dacites have peculiar trace element characteristics (Seghedi et al., 1987; Szakács et al., 1993; Mason et al., 1996; Vinkler et al., 2007; Molnár et al., 2018), characterized by an enrichment in LIL (large ion lithophile; e.g., Cs, Rb, Ba, K, Sr) and light rare earth elements and depletion in HFS (high field strength; e.g., Nb, Ti) and heavy rare earth elements (Yb, Lu, Y) with the lack of negative Eu anomaly (Eu/Eu^* values ranging from 1.21 to 0.93; Fig. 5). They are enriched in Sr and Ba (both elements show >1000 ppm).

5.2. Characteristics of the studied zircon crystals

Zircon crystals occur as inclusion in phenocrysts (mainly in plagioclase and in the felsic clots), and as microphenocrysts (30–300 μm) in the groundmass or at grain-groundmass boundaries (Fig. 6). The studied zircon crystals of the lava dome rocks are dominantly euhedral having a pale pink color, whereas zircon from pumice are colorless, glass-coated and rounded; their dimensions (i.e., length, aspect ratio) are listed in the Supplementary material. The zircon crystals, regardless of their origin (i.e., lava dome or pumice) have a restricted size range (~130–500 μm in length) compared to zircon from the peripheral domes (~110–780 μm; Molnár et al., 2018). The crystals from pumice samples are slightly more elongated than the ones from the lava dome rocks, but in general they have similar dimensional parameters (Suppl. Mat.).

5.3. Zircon U-Th ages

U-Th geochronology was applied both on crystal surfaces (i.e., rim) and interiors (i.e., mantle) in order to have input data for the disequilibrium correction (Table 2). Besides its necessity for the disequilibrium correction, these data also serve as an independent control for the (U-Th)/He dating (because the eruption age must postdate the youngest crystallization age).

In case of the pyroclastic samples, only interior ages are reported, and no measurements on the outermost crystal rims were attempted. The youngest interior crystallization ages vary between 109 ± 7 ka and 73 ± 5 ka. The average crystallization ages are uniform for the

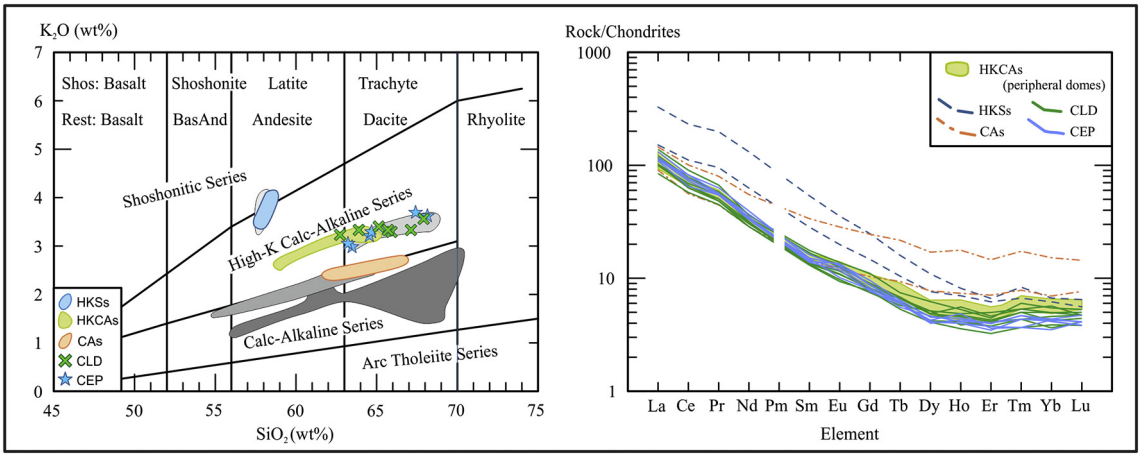

Fig. 5. Major and trace element variation of the Ciomadul dacite. SiO_2 vs. K_2O (Peccerillo and Taylor, 1976) and the REE diagram (Nakamura, 1974; Pm is not analyzed). Greyish fields indicate whole rock data of the South Harghita (dark grey: Luci-Lazu, middle grey: Cucu and Pilişca, light grey: Ciomadul) for comparison from Mason et al. (1996) and Harangi and Lenkey (2007); whereas colored ones are from Molnár et al. (2018). HKSs: high-K – shoshonitic series; HKCAs: high-K – calc-alkaline series; CAs: calc-alkaline series; CLD: Ciomadul lava dome samples; CEP: Ciomadul explosive products.

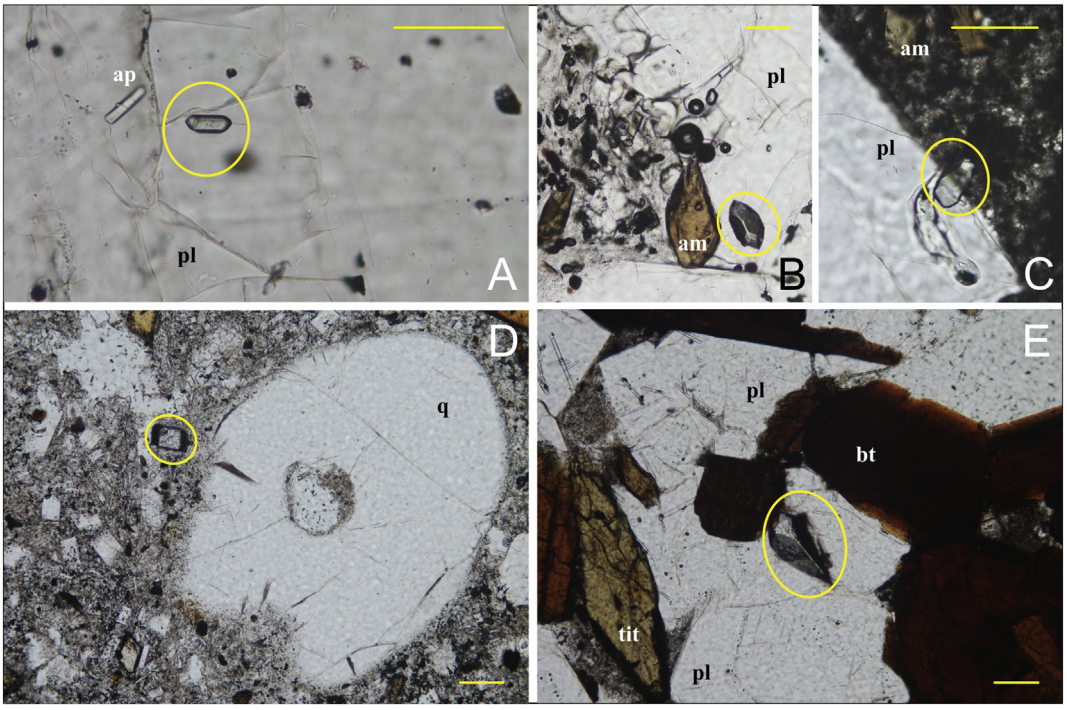

Fig. 6. Typical occurrence of the zircon crystals (yellow circles) in the Ciomadul dacite: as inclusion in plagioclase (A, B, E), at the grain-groundmass boundary (C) or in the groundmass (D). Scale bars are 100 μm; bt = biotite; ap = apatite, am = amphibole, pl = plagioclase, tit = titanite. Polarization microscopic images (1 N) from samples Haramul Ierbos (A), 205b (B), Pârâul Disznyó (DP; C) and Haramul Mare (NHM; D, E). (For interpretation of the references to color in this figure legend, the reader is referred to the web version of this article.)

Pârâul Disznyó outcrop and the 226-4b and KH-N layers (ca. 155 ka), whereas in case of the 205b location the average U-Th age is slightly younger, 125 ± 29 ka, but still overlapping within uncertainties with samples from the outcrops mentioned above.

In case of the Haramul Ierbos, Ciomadul Mic and Haramul Mare lava dome samples, rim age analyses were performed, and the youngest crystallization ages determined are 155 ± 17 ka, 142 ± 14 ka and 109 ± 10 ka, respectively. The youngest interior dates usually approach the youngest rim dates within uncertainty. The youngest interior crystallization ages vary between 192 and 115 ka, whereas the average interior crystallization ages of the lava dome samples are between 264 ± 36 ka and 157 ± 61 ka (Table 2).

Based on these average U-Th ages, the most intense phase of zircon crystallization took place between ca. 200 and 100 ka, which precedes the main lava dome construction phase, whereas only limited crystallization is recorded immediately prior to explosive eruptions (Harangi et al., 2015a).

Table 2
The average and the youngest U-Th crystallization ages of the studied samples (based on Lukács et al., 2019).

Sample name/locality		Number of data	Youngest model age (ka)	1 s (ka)	Mean age (ka)	1 s (ka)
KH-N	Interior	8	75	7	156[a]	56
226-4b	Interior	11	109	7	153[a]	34
DP	Interior	12	73	5	154[a]	48
205b	Interior	12	87	6	125[a]	29
206V	Interior	13	115	8	157[a]	61
Haramul Mare	Surface/rim	19	109	10	137	31
(NHM)	Interior	10	151	19	185[a]	23
Mohoș (MO)	Interior	29	115	8	187[a]	55
Ciomadul Mic (KCS)	Surface/rim	7	142	14	173	46
	Interior	14	143	12	191	41
Dealul Cetății (VT)	Interior	10	192	15	264[a]	36
Haramul Ierbos	Surface/rim	22	155	17	196	26
(FHM)	Interior	19	148	15	212[a]	53
Ciomadul Mare	Interior	9	184	28	226[a]	23
(NCS)						

[a] Average U-Th crystallization ages that were used for the disequilibrium correction.

5.4. Combined zircon U-Th and (U-Th)/He geochronology

Single grain zircon (U-Th)/He dating was applied to constrain the eruption history of Ciomadul volcano; detailed data are provided in the Supplementary material. Data having high uncertainty (>10%) together with those which lie outside the 95% confidence interval of the single-grain ages measured in a sample were neglected in the further calculations. The results reveal that the F_T-corrected (U-Th)/He single-grain zircon dates range between ca. 175 and 70 ka for the lava dome samples except for the dome of Piscul Pietros which yields an age range from 50 to 33 ka (n = 9) overlapping with the dated pyroclastic deposits having an age range between 58 and 36 ka.

The lava domes of Ciomadul Mare and Haramul Ierbos yielded the oldest average crystallization age-corrected (U-Th)/He zircon ages (157 ± 11 ka, n = 4 and 156 ± 18 ka, n = 11, respectively). These are overlapping with the extrusion of the Haramul Mic lava dome (154 ± 16 ka; Molnár et al., 2018). The next group comprising the lava domes of Dealul Cetății and Ciomadul Mic yielded average crystallization age-corrected (U-Th)/He ages of 137 ± 9 ka (n = 12) and 122 ± 12 ka (n = 12), respectively. The lava domes of Mohoș, Haramul Mic and the 206 V lava flow comprises the youngest group within the 150 to 90 ka time interval; their obtained average crystallization age-corrected (U-Th)/He zircon ages are 97 ± 10 ka (n = 5), 95 ± 14 ka (n = 6) and 94 ± 9 ka (n = 6), respectively. The lava dome of Piscul Pietros is distinctly younger than this lava dome building period having an extrusion age of 48 ± 6 ka (n = 9).

The eruption ages of the pyroclastic outcrops are overlapping within uncertainty with each other and also with the aforementioned Piscul Pietros lava dome. The average crystallization age-corrected (U-Th)/He zircon ages are 55 ± 5 ka (n = 6) for the 205b deposit, 53 ± 5 ka (n = 5) for the lower part of the 226 deposit (226c layer), and 51 ± 5 ka (n = 5) for the Pârâul Disznyó location. The correction for disequilibrium at the time of eruption in case of the 226c deposit was based on

the published average zircon crystallization age of the identical KH-A deposit (152 ± 14 ka; Harangi et al., 2015a), due to the low amount of zircon crystals suitable for dating from the sample 226c. The upper layers of both the KH and 226 deposits (226-4b and KH-N layers) revealed slightly younger ages than the lowermost ones, although these ages overlap within uncertainty. Their average crystallization age corrected (U-Th)/He zircon ages are 48 ± 13 ka (n = 5; 226-4b) and 45 ± 7 ka (n = 3; KH-N).

Double-dating was performed for zircon crystals of the Haramul Ierbos and Ciomadul Mic lava domes (Fig. 7, Suppl. mat.). The error-weighted average ages are 157 ± 11 ka (n = 7, goodness of fit: 0.352) for the Haramul Ierbos lava dome and 133 ± 8 ka (n = 3, goodness of fit: 0.995) for the Ciomadul Mic lava dome which are overlapping within uncertainty with their average crystallization age corrected ages.

5.5. Lava dome volume calculations

Karátson and Tímár (2005) and Szakács et al. (2015) published lava dome volumes to better constrain regional eruption rates. We performed additional calculations (Fig. 8) whereby volumes were obtained not just for those lava domes which eruption ages are presented here, but also for the older phase of the Ciomadul volcanic dome field and the Murgul Mare lava dome (Molnár et al., 2018) to obtain a comprehensive data set for the volumes of eruptions over the past ca. 2 million years. Defining the boundaries of Ciomadul Mic and Ciomadul Mare was hampered by the composite structure of the volcano, and therefore both are included with the "Ciomadul cluster" along with Dealul Cetăţii, Vârful Surduc, Vârful Comloş and Dealul Taţa domes (Fig. 8). The spatial extent of the Haramul Mare and Haramul Ierbos lava domes is also poorly defined and volume estimates are tentative.

6. Discussion

6.1. Resolution of the eruption ages

Combined zircon U-Th and (U-Th)/He dating permits constraining eruption ages for Late Pleistocene to Holocene volcanic eruptions, even though zircon crystallization typically predates the eruption (Danišík et al., 2017). Moreover, the youngest zircon rim/surface U-Th ages provides a maximum limit for the eruption, and the U-Th crystallization ages can be used to correct the disequilibrium in the U-decay chain (Farley, 2002; Farley et al., 2002; Schmitt et al., 2006). However, there are still some ambiguities in determining accurate (U-Th)/He eruption ages. The main biasing factors are uncertainties in the F_T–correction, mainly due to the unknown parent nuclide distribution, and crystallization age heterogeneity in the dated crystals (e.g., Hourigan et al., 2005; Bargnesi et al., 2016).

Here, we explore two approaches for the disequilibrium correction, each with their own advantages and disadvantages: using an average crystallization age, or double-dating of crystal rims coupled with bulk analysis of (U-Th)/He ages (e.g., Schmitt et al., 2006, 2010; Danišík et al., 2012, 2017; Molnár et al., 2018). In the first case, the correction is performed by using the weighted-average of U-Th zircon interior ages, typically derived from a different set of crystals as used for (U-Th)/He dating (e.g., Schmitt et al., 2006; Danišík et al., 2012; Harangi et al., 2015a; Molnár et al., 2018). In the second case U-Th zircon rim ages are determined first, and the same crystals are subsequently analyzed for (U-Th)/He, preferentially targeting those with the oldest U-Th ages and thus the smallest disequilibrium corrections (Schmitt et al., 2010). However, when old U-Th zircon rim ages are scare or absent, there is a chance for overestimating the true eruption age by applying a correction based on the zircon rim crystallization age, whereas the crystal interior, which yield most of the analyzed ^{4}He, might be older and thus require a smaller disequilibrium correction (Schmitt et al., 2014). Despite these ambiguities, determining the U-Th zircon rim age can provide an independent maximum eruption age control (i.e., the eruption age cannot be older than the youngest rim age), an important information which is less stringent if only the interior U-Th zircon ages are determined. Studies applying both methods showed that the eruption ages determined by the different corrections are usually overlapping with each other within uncertainty (e.g., Danišík et al., 2012; Molnár et al., 2018). Error-weighted average ages where uncertainties of individual (U-Th)/He zircon analyses are based on the minima and maxima of permissive disequilibrium corrections can be used to mitigate effects of a potential overestimation during the double-dating method (e.g., Schmitt et al., 2014), and this is what

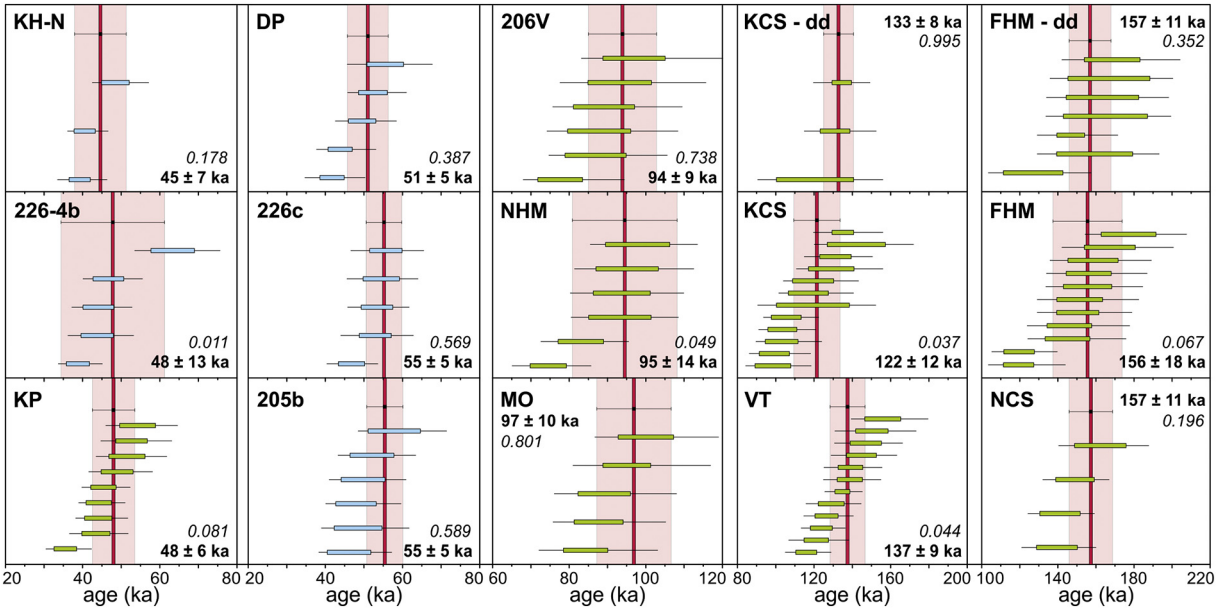

Fig. 7. Disequilibrium-corrected zircon (U-Th)/He ages of the dated lava dome samples (green) and pyroclastic outcrops (blue). The eruption ages (red bars; bold numbers) are presented with 2σ*√MSWD uncertainties in case of the average crystallization age correction, and with 2σ in case of the double-dating samples (KCS-dd, FHM-dd). For the latter, eruption ages were computed as error-weighted average ages. The lower and upper end of each (green and blue) bar represent the secular equilibrium (minimum) and the disequilibrium corrected (maximum) (U-Th)/He age of the dated zircon crystal. Goodness-of-fit values are represented for each sample panel in italic. (For interpretation of the references to color in this figure legend, the reader is referred to the web version of this article.)

Locality	height of perimeter (m)	area (km²)	volume from surface data (km³)	reference
Murgul Mare	776	0.8	0.10	this study
Pilişca[a]	*635**	*123.1*	*17.4*	*Karátson and Timár (2005)*
Baba-Laposa	676	1.8	0.21	this study
Dealul Mare	766	2.0	0.33	this study
Dealul Mare	*nd*	*1.5*	*0.57*	*Szakács et al. (2015)*
Puturosul	*nd*	*0.3*	*0.17*	*Szakács et al. (2015)*
Bálványos	*nd*	*0.1*	*0.07*	*Szakács et al. (2015)*
Haramul Mic	747	1.1	0.15	this study
Haramul Mic	*nd*	*1.3*	*0.34*	*Szakács et al. (2015)*
"Haramul cluster"[b]	793	3.3	0.62	this study
Haramul Mare dome cluster[b]	*nd*	*5.3*	*2.28*	*Szakács et al. (2015)*
Haramul Ierbos	959	0.5	0.06	this study
Haramul Mare	778	1.7	0.29	this study
Mohoş	884	1.2	0.19	this study
"Ciomadul cluster"[c]	634	13.6	4.13	this study
Ciomadul Mare dome cluster[c]	*nd*	*9.7*	*4.22*	*Szakács et al. (2015)*
Dealul Cetăţii	718	1.2	0.20	this study
Piscul Pietros	*nd*	*1.1*	*0.47*	*Szakács et al. (2015)*
volcanoclastic	*nd*	*62.4*	*0.62*	*Szakács et al. (2015)*
Ciomadul (in total)[d]	*650**	*80.9*	*12.2*	*Karátson and Timár (2005)*

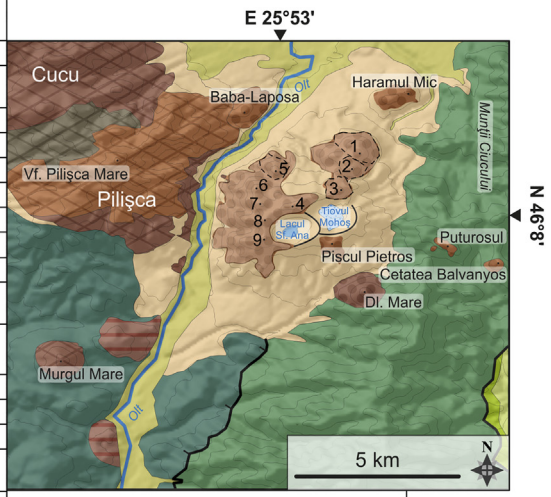

*average height of perimeter (m)
a: Pilişca volcanic edifice in total together with Baba-Laposa
b: Haramul Mare, Haramul Ierbos and Mohoş lava domes
c: Ciomadul Mare, Dealul Cetăţii, Vârful Surduc, Vârful Comlos, Ciomadul Mic, Dealul Taţa
d: Ciomadul volcanic complex together with the peripheral lava domes
nd: no data available

Fig. 8. Results of the lava dome volume calculations (DRE) supplemented with the previous results (left panel) and the boundaries of the domes on the geological map (right panel) which were used for the calculations.

we apply in this study resulting in approximate eruption age uncertainties of 10–30%. We emphasize that these error estimates are conservative, and because of the systematic relationship between (U-Th)/He zircon eruption ages always being younger than U-Th zircon crystallization ages, these ages are robust within stated uncertainties.

Combined zircon U-Th and (U-Th)/He eruption ages of the tephra deposits related to the explosive activity of Ciomadul volcano serve as a good example to test the resolution limits of the applied dating method – i.e., in what scale and how detailed distinct mapped eruption units can be temporally resolved. Here and in previous studies, nine pyroclastic deposits were dated in total (Vp, Bx, Tf, KH-A; 201b; 202: Harangi et al., 2015a, 2018; 226c, 226-4b, KH-N, 205b, DP: this study; Figs. 1, 2; Table 1) which represent most of the present-day known pyroclastic deposits of the Ciomadul volcano.

Unfortunately, there are only a few cases where the same pyroclastic deposit can be clearly identified in different exposures around the volcano. Thus, due to the isolated outcrop situation, it is generally impossible to uniquely trace individual eruption events throughout different stratigraphic sections. An exception is the samples KH and 226 which were collected from outcrops at the eastern slope of the volcano and the northeastern crater rim of the Mohoş crater, respectively (Figs. 2, 4). Here, both sections show thick pumiceous pyroclastic deposits near the bottom and a coarser-grained pumiceous bed near the top. We obtained ages of 55 ± 5 ka and 56 ± 5 ka for the bottom layers (226c: this study; KH-A/"MK-4": Harangi et al., 2015a, respectively) and 48 ± 13 ka and 45 ± 7 for the top layers (226-4b and KH-N, respectively) at both locations. These ages corroborate that both sequences record the same eruption events (Figs. 7, 9, 10). The 7–10 kyr difference in the eruption ages between bottom and top might indicate that these sections record a hiatus between individual pyroclastic deposits, but ages overlap within uncertainty.

In addition to the deposits cropping out at sampling localities 226 and KH, this explosive eruption stage involves additional locations (205b, DP, KP and Tf; Figs. 2, 9). These represent lava dome extrusions (KP), block-and-ash flow deposits likely resulting from lava dome collapse (205b, DP), and a series of pyroclastic fall and subsequent flow

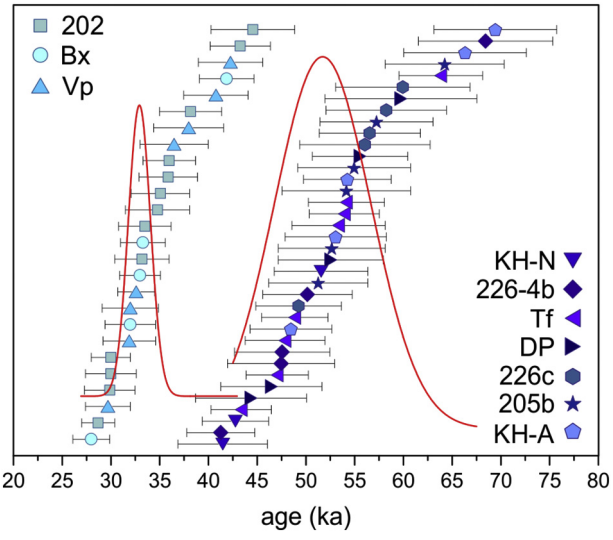

Fig. 9. Ranked-order plot of the individual disequilibrium-corrected zircon (U-Th)/He ages from the pyroclastic samples. The dated pyroclastic deposits (Bx, Vp, Tf, KH-A, 202: Harangi et al., 2015a; KH-N, 226-4b, DP, 226c, 205b: this study) suggest by the unequal variances *t*-test two major eruptive pulses at ca. 52 ka (blue) and 33 ka (green). However, further subdivision within the two groups cannot be performed. Red curves are the probability density plots of the two groups (Suppl. Mat.). (For interpretation of the references to color in this figure legend, the reader is referred to the web version of this article.)

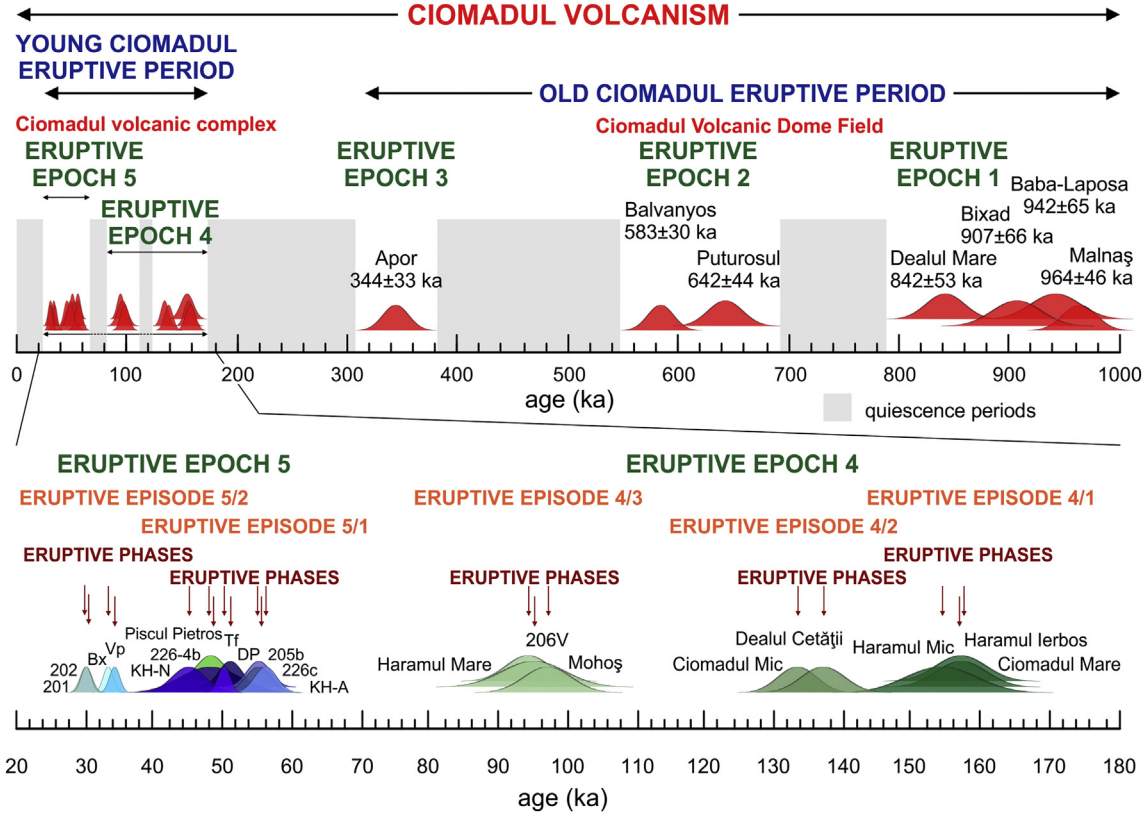

Fig. 10. Volcanic activity units of the Ciomadul volcanism based on the division scheme of Fisher and Schmincke (1984), refined further by Lucchi (2013). Eruption ages are supplemented with data reported in Harangi et al. (2015a) and Molnár et al. (2018).

events (Tf) associated with larger explosive eruptions. Eruption ages are overlapping within uncertainty (including KH and 226 eruption ages; Figs. 7, 9) and therefore, no further subdivision is possible according to our data. Nevertheless, the combined zircon U-Th and (U-Th)/He eruption ages clearly define an eruptive episode between 55 and 45 ka, starting with voluminous explosive eruptions. We thus reconfirm the results of Harangi et al. (2015a) that the entire pyroclastic section of the Bolondos Hill outcrop (KH in this study; BOL-1 in Karátson et al., 2016) belongs to this eruption stage, and not to a younger event as suspected by Karátson et al. (2016) based on compositional grouping of glass shard analysis results. Using additional zircon dating, we corroborated the age of the Piscul Pietros (KP; 48 ± 6 ka in this study, whereas Harangi et al., 2015a published 43 ± 2 ka), since the difference is within the uncertainty and it remained within the same eruption stage.

Based on the unequal variances t-test, a younger age cluster can be resolved comprising Vp, Bx, 202 and 201b pyroclastic deposits (Harangi et al., 2015a, 2018; Figs. 1, 2, 9). This ultimate eruption stage has an age range of 34.0–29.5 ka (Harangi et al., 2015a, 2018) and appears to have occurred after several thousand years of quiescence following the older explosive stage (Fig. 10). This youngest eruption stage involved two large, explosion crater-forming events (Sf. Ana crater) with different petrologic and compositional characters. They yielded relatively thick distal pyroclastic deposits at >20 km distance from the crater (sampling locations 201b and 202; Vinkler et al., 2007; Harangi et al., 2015a, 2018; Karátson et al., 2016).

6.2. Eruption chronology

The very detailed eruption dating by combined zircon U-Th-Pb and (U-Th)/He method presented in Harangi et al. (2015a), Molnár et al. (2018) and this paper enables us to develop a conceptual model for the eruptive history for the entire Ciomadul volcanism. This is fundamental to understand the behavior of a volcanic system which could be a base of further evaluation of its volcanic hazards. The principle of this model is the volcanic activity unit-based nomenclature proposed by Fisher and Schmincke (1984) and applied subsequently for Italian volcanoes by Francalanci et al. (2013) and Lucchi (2013). This eruption history concept can be connected with the lithostratigraphic unit-based classification, which is based on detailed mapping of the volcanic stratigraphy (Gropelli and Viereck-Goette, 2010). The eruption history nomenclature put forward by Fisher and Schmincke (1984) uses the duration of continuous volcanic activity and the repose time between the eruptions. In our case the relatively large uncertainties (a few kyr) of the determined eruption ages do not permit to distinguish single eruption events and pulses that may last from minutes to days to decades. Thus, the smallest unit is the eruption phase which is defined here by a dated eruption as preserved in its mappable volcanic products. An eruption phase may represent a complex eruption event, e.g., a block-and-ash flow deposit, may be the result of protracted lava dome growth and collapse events, or a set of Vulcanian explosions associated with fountain collapse. Ages of successive eruption phases often overlap each other within their uncertainties and thus, they cannot be clearly separated from one another unless they are superimposed in outcrop. However, such a situation is quite rare in Ciomadul (an example of this is the volcanic layers of KH and 226 outcrops). Overlapping eruption phases can form an eruption episode. The length of the eruption episode can be determined by its youngest and oldest eruption phases and it is usually a few thousand years. Lucchi (2013) suggested that an eruptive epoch could be defined as a period of volcanic activity with duration over thousands of years developing an independent volcano. Between the eruptive epochs, significant changes could occur during quiescence, such as important tectonic event(s), substantial shifting of the eruptive vents and/or remarkable change of the magma composition. Here, we define the eruption epochs based on extended (several 10s kyr) quiescence intervals.

Thus, the ca. 1 Myr-long Ciomadul volcanism is divided into two main stages, which differ largely in their style of volcanic activity: initially scattered small-volume lava domes developed separated by long repose times and resulting in a volcanic dome field. Then the eruption centers focused into a more restricted area and the eruptions built the Ciomadul volcanic complex with much higher eruption flux. Thus, we define an Old Ciomadul Eruptive Period (OCEP) from 1 Ma to 300 ka followed by the Young Ciomadul Eruptive Period (YCEP) from 160 ka to 30 ka (Fig. 10).

During the OCEP lava dome extrusions occurred in three stages (Fig. 10). The Malnaş, Baba-Laposa, Bixad and Dealul Mare lava domes were formed between 1 Ma and 800 ka (Molnár et al., 2018). Overlapping uncertainties (±46–66 ka) of the combined zircon U-Pb and (U-Th)/He eruption ages preclude further subdivision of this eruptive epoch (Eruptive Epoch 1; Fig. 10). After about 100 kyr of quiescence, two lava domes were built at the eastern part of the volcanic dome field: Puturosul and Balvanyos with slightly different ages, which however, overlap within uncertainties (642 ± 44 ka and 583 ± 30 ka, respectively; Molnár et al., 2018). These comprise Eruptive Epoch 2 (Fig. 10). After another >100 kyr of repose time, the Apor lava flow occurred at 344 ± 33 ka. We do not know any other eruption events at that time, although we cannot exclude that such deposits are covered by subsequent lava domes of the Ciomadul. Thus, the Eruption Epoch 3 contains only one single eruption based on our present knowledge.

Construction of the Ciomadul volcanic complex during the YCEP occurred between 160 and 30 ka by amalgamation of several lava domes followed by an explosive volcanic stage resulting in twin-craters (Figs. 10, 11). We found a relatively long (ca. 40 kyr) repose time between the lava dome extrusion stage (160–90 ka) and the younger, mostly explosive volcanic stage (55–30 ka). Thus, we divided them into Eruptive Epoch 4 and 5 (Fig. 10). Eruptions took place more frequently during these epochs compared to the OCEP (Fig. 10). So far, we dated eight extrusive events within the 70 kyr-long Eruptive Epoch 4 tentatively grouped into three Eruptive Episodes separated by a few kyr of quiescence (Fig. 10). The peripheral Haramul Mic (KHM; 154 ± 16 ka; Molnár et al., 2018) formed coeval with the lava domes of Ciomadul Mare (NCS) and Haramul Ierbos (FHM; Eruptive Episode 4/1 at ca. 155 ka; Fig. 10). Thus, at least three separate eruptive centers were active at that time (Fig. 11). Ciomadul Mic (KCS) developed close to the Ciomadul Mare dome, but is ca. 20 kyr younger and overlaps in age with the Dealul Cetații lava dome (VT; Eruptive Episode 4/2 at ca. 135 ka; Fig. 10). The age difference between Ciomadul Mic and Ciomadul Mare is corroborated by their distinct petrologic characters (Kiss et al., 2014). The youngest lava dome cluster (Eruptive Episode 4/3 at ca. 95 ka; Fig. 10) involves the Haramul Mare (NHM) and Mohoş (MO) lava domes and a lava flow (206 V) mapped at the southern slope of the Ciomadul volcanic complex (Fig. 2). Although an apparent ca. 40 kyr gap can be observed between the Eruptive Episodes 4/2 and 4/3, there are still undated domes within the volcanic complex which could either fill this gap or be part of one of the Eruptive Episodes (4/1, 4/2 or 4/3). Therefore, we classified all the lava domes formed between 160 and 90 ka into the Eruptive Epoch 4 which could be refined by further geochronological data. The alignment of the contemporaneously formed domes at 155 ka, 135 ka and 95 ka follows a NE-SW direction which parallels the alignment of ca. 1 Ma lava domes of Baba-Laposa, Bixad and Malnaş perpendicular to the general NW-SE direction of the Călimani-Gurghiu-Harghita volcanic chain. This NE-SW trend also parallels the nappe boundary of the Cretaceous flysch deposits (Fig. 11; Szakács et al., 2015) suggesting that this fault/nappe boundary could be a possible pathway for the ascending magmas.

Based on our age determinations, we can recognize a gap of about 40 kyr between the initial lava dome extrusions and the youngest eruption stage and therefore, the youngest eruptions are grouped into a separate eruptive epoch (Eruptive Epoch 5; Fig. 10). It comprises mostly explosive volcanic deposits although coeval lava dome formation is not ruled out. This is supported by the presence of block-and-ash flow deposits which may be related to dome collapse events, and also the jointed blocks with glassy rinds which are abundant in ravines at the southern slope of the volcano. In addition, the Piscul Pietros (KP) lava dome at the southern crater rim of the Sf. Ana-Mohoş craters represents the youngest preserved extrusive rocks of this epoch (48 ± 6 ka). The explosive volcanism appears to have taken place during two Eruptive Episodes separated by few kyr of quiescence (Fig. 10). The latest eruptions (Eruptive Episode 5/2) were particularly violent involving Vulcanian and sub-Plinian as well as strong phreatomagmatic eruptions resulting in relatively thick (>20 cm) distal tephra layers >20 km from the volcano (Vinkler et al., 2007; Harangi et al., 2015a; Karátson et al., 2016). This occurred at 30–32 ka and since that time the volcano is again in a quiescence period.

The final eruption centers (i.e., the two craters) are situated on the jointing of the two lineaments – i.e., the NW-SE general trend of the Călimani-Gurghiu-Harghita volcanic chain and the NE-SW trend of the main lava domes.

The long-lasting history of volcanism (ca. 1 Myr) and the long repose times (up to 100 kyr) between the active phases of Ciomadul are not rare in andesitic-dacitic volcanoes worldwide (e.g., Wörner et al.,

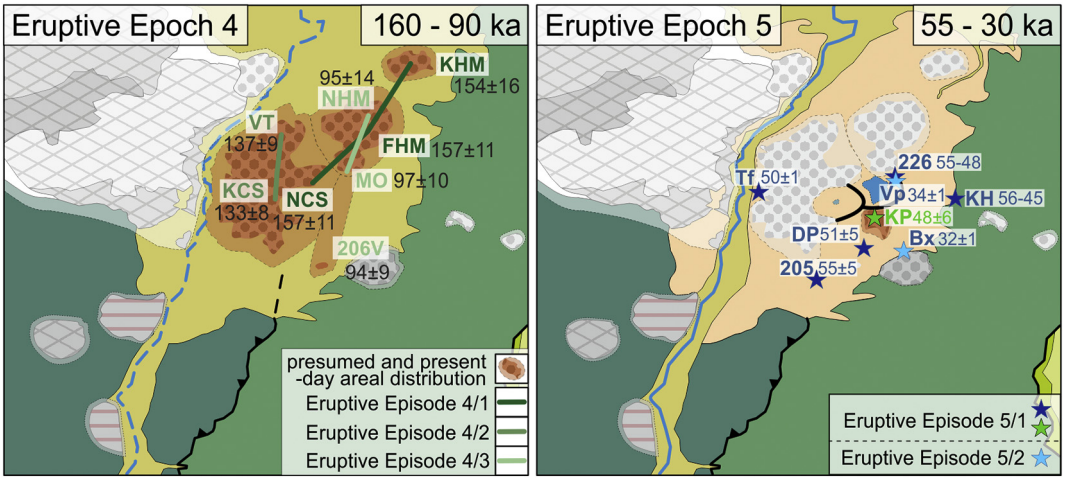

Fig. 11. Spatial distribution of the supposed studied eruption centers and pyroclastic deposits of the Ciomadul Volcanic Dome Fields for the 160–90 ka (left panel) and 55–30 ka (right panel) time interval (ages in ka). Besides the base map, colored fields are indicating the volcanological active areas within the two periods. The trends of the coeval volcanic activities within Eruptive Epoch 4 are perpendicular to the normal NW-SE trend of the chain. The two excavated craters which were formed during Eruptive Epoch 5 are situated at the jointing of the two perpendicular trends. Color coding is the same as in Figs. 2 and 10. The volcanologically not active areas are marked by greyish color, whereas the black dashed line is the possible continuation of the reverse fault (left panel).

2000; Klemetti and Grunder, 2008). Hildreth and Lanphere (1994) emphasized the importance of comprehensive geochronological studies coupled with stratigraphic, geochemical and petrologic data to reveal the details of eruption frequency of such volcanoes. Based on high-precision K-Ar dating, they could reveal a 30 kyr of quiescence during the evolution of Mount Adams volcanic field. Subsequent studies corroborated that such long hiatus could commonly occur in the lifetime of a volcanic system (e.g., Andes: Tatara-San Pedro; Singer et al., 1997; Parinacota; Hora et al., 2007; Tungurahua; Bablon et al., 2018; Mexican volcanic belt: Ceboruco-San Pedro; Frey et al., 2004; Tequila; Lewis-Kenedi et al., 2005; Cascades: Lassen Peak; Clynne and Muffler, 2010; Mt. Adams; Hildreth and Lanphere, 1994). The Ciomadul Volcanic Dome Field shows the same characteristic having long repose times during the eruption history; although it has much less erupted volume compared to the abovementioned volcanic fields. Furthermore, the compositional homogeneity of the erupted magmas is also notable which resembles the behavior of Taapaca in Central Andes, where monotonous silicic andesite-dacite erupted for a prolonged (ca. 1.2 Myr) period (Clavero et al., 2004). Understanding the reason of recurrence of volcanic activity after a long quiescence is fundamental to evaluate the potential hazard in seemingly inactive volcanic regions. This depends primarily on the state of magma storage beneath these volcanoes. While the sharp change in composition of the erupted magma after a long hiatus could indicate a major reorganization in the magma storage and possible ascent of new magma batches from deeper hot zone (e.g., Parinacota, Andes; Hora et al., 2007), the monotonous magma composition could imply long standing crystal mush storage with intermittent rejuvenation of its certain parts (e.g., Lassen Peak, Cascades; Klemetti and Clynne, 2014). The Ciomadul resembles the latter, Lassen Peak example corroborated also by the zircon U-Pb and U-Th crystallization ages suggesting a prolonged magma storage existence (Harangi et al., 2015a; Lukács et al., 2018b, 2019). The commonly found long repose times between the active phases suggest that the nature of a volcano cannot be understood solely based on the elapsed time since the last eruption. Instead, comprehensive geochronology, coupled with the understanding of the magma storage behavior could be a base of hazard assessment even in volcanic fields, where the last eruptions occurred several 10s of thousand years ago and therefore they are not considered as potentially active.

6.3. Magma output rates and implications on the eruptive behavior

The detailed timescale of the eruption history for Ciomadul also enables characterization of the eruption rate of the volcano. The amount of erupted magma in the Călimani-Gurghiu-Harghita volcanic chain decreases as eruption centers become younger and migrate towards the southeast (Seghedi et al., 1995; Szakács and Seghedi, 1995; Karátson and Tímár, 2005). The Ciomadul Volcanic Dome Field is the youngest and southeasternmost end-member, and also the smallest dome field within the chain. At the Ciomadul volcanic dome field, a large decrease in the amount of erupted materials occurred at ca. 1 Ma, in addition to the change in geochemical affinity from normal to high-K – calc-alkaline (Mason et al., 1996; Molnár et al., 2018). Previous studies for the 2.1–1.6 Ma Pilişca volcano calculated 17.4 km^3 of erupted material, with an eruption rate of 0.02 km^3/kyr (Karátson and Tímár, 2005). After the ca. 600 kyr of quiescence, the volumes of the 1–0.3 Ma high-K – calc-alkaline lava domes (Baba-Laposa, Dealul Mare, Puturosul, Bálványos, Turnul Apor) did not exceed 1.0 km^3 (Szakács et al., 2015; this study) resulting in a very low eruption rate (~0.001 km^3/kyr; Fig. 12) for the OCEP.

After the last 100 kyr of quiescence, when the main part (~6 km^3) of the Ciomadul volcanic complex formed (160–90 ka), the eruption rate and volume increased, reaching its peak eruption rate of 0.1 km^3/kyr during Eruptive Epoch 4. Despite the evident increase of eruption rate, magma composition remained invariant throughout this period with younger domes having the same high-K – calc-alkaline character as the older (1–0.3 Ma) domes (Fig. 5). The last phase of activity is characterized by mainly explosive eruptions between 55 and 30 ka. Volume calculations for this period were not possible due to the dense vegetation of the area. The YCEP has a higher eruption rate (~0.05 km^3/kyr; Fig. 12) and shorter quiescence periods compared to the OCEP, and characterized by the formation of the main lava dome complex, the two craters and the volcanoclastic/pyroclastic deposits covering the flanks.

Volcanoes erupting in present-day continental subduction zones (e.g., Cascades, Andes; e.g., Hildreth and Lanphere, 1994; Lewis-Kenedi et al., 2005; Klemetti and Grunder, 2008; Samaniego et al., 2012; Bablon et al., 2018) are generally characterized by a larger amount of eruptive material (generally ≫ 10 km^3), higher eruption rates (0.5–0.7 km^3/kyr) and a more heterogeneous geochemical composition (from basalts, basaltic andesites to rhyolites). Ciomadul Volcanic Dome Field displays similarities with these types of volcanoes mainly with regard to the overall longevity (ca. 1 Myr; e.g., Aucanquilca, Andes; Klemetti and Grunder, 2008), the protracted quiescence periods (e.g., Tungurahua, Andes; Bablon et al., 2018), and a continuous zircon crystallization history (e.g., Lassen Peak, South Cascade Range; Klemetti and Clynne, 2014). The 0.1 km^3/kyr eruption rate of the 160–90 ka period and the 0.05 km^3/kyr eruption rate of the YCEP overall are also comparable to the low-production eruption stages of some of the continental arc-volcanoes (e.g., Chimborazo, Samaniego

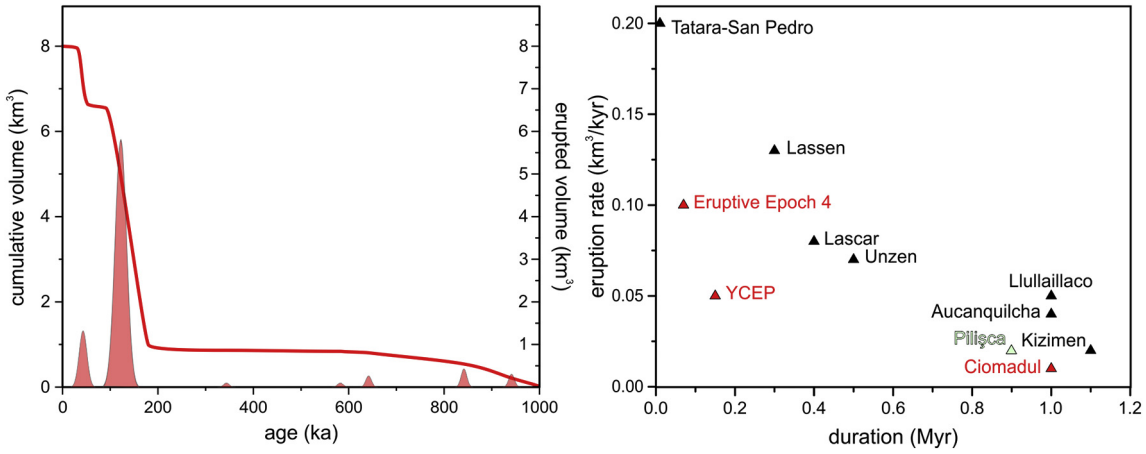

Fig. 12. Cumulative eruption volume and erupted volumes vs time (left panel) and a comparison with other dacitic volcanoes (right panel; after Klemetti and Grunder, 2008); lava dome volume data are supplemented with previous volumes reported in Karátson and Tímár (2005) and Szakács et al. (2015). YCEP = Young Ciomadul Eruptive Period; Ciomadul = Ciomadul volcanic dome field.

et al., 2012; Mt. Adams, Hildreth and Lanphere, 1994). The total eruption rate of ~0.01 km^3/kyr for the long-lived (ca. 1 Myr) Ciomadul volcanic dome field is in line with other long-lived dacitic volcanoes such as Aucanquilcha or Kizimen (Klemetti and Grunder, 2008), although these have somewhat higher eruption rates (Fig. 12). Another common characteristic of the eruptive behavior of these dacitic volcanoes (i.e., starting with a larger eruption rate which declines in time; Klemetti and Grunder, 2008) can also be seen at Ciomadul if we consider only the Young Ciomadul Eruptive Period (Fig. 12). However, for the entire Ciomadul volcanism quite the opposite can be observed i.e., a very low eruption rate at the beginning (~0.001 km^3/kyr; OCEP) with a large increase for the younger period (~0.05 km^3/kyr; YCEP; Fig. 12).

Despite the large number of similarities with continental arc magmatism, Ciomadul is situated in a post-collisional geodynamic setting (Seghedi et al., 2011). It therefore features distinct properties such as an eruptive focus on regional tectonic lineaments and high-K geochemical compositions which are common in volcanic areas in post-collisional settings (e.g., Halloul and Gourgaud, 2012; Ghalamghash et al., 2016; Kasapoğlu et al., 2016). The lower total erupted amounts and the smaller eruption rates of Ciomadul compared to other dacitic volcanoes can be possibly explained by its different tectonic setting. The post-collisional setting and the peculiar geometry of Ciomadul (i.e., it overlays the flysch deposits of the Carpathian collision zone) could have had a large control on the magma generation and a high effect on the erupted amounts especially during the initial activity (ca. 1–0.3 Ma). As the system evolved (i.e., enlarged), higher amount of magmas could reach the surface, thus forming the main lava dome complex of Ciomadul (ca. 160–30 ka). However, even during this more productive stage (YCEP), several long repose times (up to tens of kyr) occurred between the eruptions (Fig. 10). This eruptive behavior, coupled with the present-day state of a subvolcanic magma storage and the presence of the regional still active tectonic lineaments are the most crucial information which needs to be taken into account for hazard assessment of Ciomadul and similar volcanoes worldwide.

7. Conclusion

Combined zircon U-Th and (U-Th)/He dating was used to build up a comprehensive geochronological framework for the Late Pleistocene volcanism of the Ciomadul volcanic complex, the youngest volcano of eastern Europe. This method is proven to be powerful to constrain the eruption ages when other suitable mineral phases for dating are lacking. The new results, supplemented with eruption ages published by Harangi et al. (2015a) and Molnár et al. (2018), reveal the phases of volcanic activity and quiescence periods and enable us to develop a conceptual model for the volcanism of the Ciomadul volcanic dome field (1 Ma–30 ka).

The initial eruption phase, denoted as Old Ciomadul Eruptive Period (1 Ma–300 ka; OCEP) was characterized by intermittent eruptions separated by long (>100 kyr) repose times. At ca. 160 ka, a major change occurred and during the Young Ciomadul Eruptive Period (160–30 ka; YCEP) a remarkably larger amount of magmas erupted and built up the main lava dome complex of Ciomadul. Both the OCEP and the YCEP can be further subdivided into eruptive epochs. Within the YCEP, the eruption ages of the lava domes revealed that the main lava dome forming activity (Eruptive Epoch 4) occurred in three eruptive episodes at ca. 155 ka (Eruptive Episode 4/1: Ciomadul Mare, Haramul Ierbos, Haramul Mic), 135 ka (Eruptive Episode 4/2: Dealul Cetății, Ciomadul Mic) and 95 ka (Eruptive Episode 4/3: Mohoș, 206 V, Haramul Mare). Vent alignment of these three episodes follows a NE-SW trend perpendicular to the regional NW-SE trend presented by the volcanic edifices of the Călimani-Gurghiu-Harghita volcanic chain.

After ca. 40 kyr of quiescence, a major change in the eruption style occurred during the Eruptive Epoch 5 of the YCEP between 55 and 30 ka. This volcanic stage was characterized by mostly explosive eruptions in addition to lava dome extrusions. The Eruptive Episodes 5/1 and 5/2 can be distinguished based on the previously published data (Harangi et al., 2015a) and this study. The pyroclastic deposits and also the lava dome of Piscul Pietros which were dated during this study belong to the Eruptive Episode 5/1 having an eruption age ca. 55–45 ka, whereas the Eruptive Episode 5/2 which is the youngest volcanic activity in the entire Carpathian-Pannonian Region occurred at ca. 30 ka. The eruption centers active during these two ultimate eruptive episodes are situated at the junction of the previously defined NW-SE and NE-SW lineaments.

This comprehensive geochronological study revealed long quiescence periods between the active volcanic phases. The well-constrained long repose times in the history of many volcanoes warn that the nature of volcanoes cannot be evaluated only by the elapsed time since the last eruption. Potentially active volcanoes are usually defined for those, which erupted within the last 10 ka (Siebert et al., 2011). However, geochronological studies suggest that volcanic eruption could occur even after several 10s of kyr of quiescence. Thus, the capability for a volcano to erupt again depends primarily on the state of the subvolcanic magma storage rather than the length of the repose time. If a melt-bearing magma storage can be detected beneath a long-dormant volcano, the potential of reawakening cannot be excluded. This led Harangi et al. (2015a, 2015b) to propose the term PAMS volcano for those volcanoes which had their ultimate eruption >10 ka, but there are observations for the existence of a melt-bearing subvolcanic magmatic system.

Based on the new eruption ages and additional estimates for eruptive volume of certain lava dome edifices of the Ciomadul Volcanic Dome Field, we could refine magma output rates. The maximum eruption rate was reached during Eruptive Epoch 4 (the main lava dome building stage) with 0.1 km^3/kyr, although this is still substantially lower than for volcanoes at continental arc settings. This might be explained by the post-collisional setting of Ciomadul that requires tectonic control of eruptive behavior.

Acknowledgement

The research was financed by the Hungarian National Research, Development and Innovation Fund (NKFIH) within No. K116528 and PD 121048 projects; and supported by the European Union and the State of Hungary, co-financed by the European Regional Development Fund in the project of GINOP-2.3.2-15-2016-00009 'ICER'. K. Molnár was subsidized by the Talented Student Program of the Eötvös Loránd University (Budapest, Hungary) and by the Campus Hungary Short Term Study Program (Balassi Institute). B. Kiss was supported by National Research, Development and Innovation Found of Hungary, financed under PD 120891. I. Seghedi benefited by a grant of the Ministry of Education and Scientific Research, CNCS-UEFISCFI, projects PN-II-IDPCE-2012-4-0137 and PN-III-P4-ID-PCCF-2016-0014. Ion microprobe facilities at UCLA and Heidelberg University acknowledge funding through NSF Instrumentation and Facilities, and DFG Scientific Instrumentation and Information Technology programs, respectively. The invaluable help of Judit Dunklné Nagy (Göttingen, Germany) during the (U-Th)/He measurements is very much appreciated. The authors thank the members of the MTA-ELTE Volcanology Research Group (Budapest, Hungary) for their helps during the field and laboratory works. We thank Joan Marti for the editorial helping and the two anonymous reviewers for the constructive comments.

Appendix A. Supplementary data

Supplementary data to this article can be found online at https://doi.org/10.1016/j.jvolgeores.2019.01.025.

References

Bablon, M., Quidelleur, X., Samaniego, P., Le Pennec, J.-L., Lahitte, P., Liorzou, C., Bustillos, J.E., Hidalgo, S., 2018. Eruptive chronology of Tungurahua volcano (Ecuador) revisited based on new K-Ar ages and geomorphological reconstructions. J. Volcanol. Geotherm. Res. 357, 378–398. https://doi.org/10.1016/j.jvolgeores.2018.05.007.

Bargnesi, E.A., Stockli, D.F., Hourigan, J.K., Hager, C., 2016. Improved accuracy of (U-Th)/He zircon ages by rectifying parent nuclide zonation with practical methods. Chem. Geol. 426, 158–169. https://doi.org/10.1016/j.chemgeo.2016.01.017.

Clavero, J.E., Sparks, R.S.J., Pringle, M.S., Polanco, E., Gardeweg, M.C., 2004. Evolution and volcanic hazards of Taapaca Volcanic Complex, Central Andes of Northern Chile. J. Geol. Soc. 161, 603–618. https://doi.org/10.1144/0016-764902-065.

Clynne, M.A., Muffler, L.J.P., 2010. Geologic Map of Lassen Volcanic National Park and Vicinity, California: U.S. Geological Survey Scientific Investigations Map 2899, Scale 1: 50,000.

Danišík, M., Shane, P., Schmitt, A.K., Hogg, A., Santos, G.M., Storm, S., Evans, N.J., Keith Fifield, L., Lindsay, J.M., 2012. Re-anchoring the late Pleistocene tephrochronology of New Zealand based on concordant radiocarbon ages and combined $^{238}U/^{230}Th$ disequilibrium and (U–Th)/He zircon ages. Earth Planet. Sci. Lett. 349–350, 240–250. https://doi.org/10.1016/j.epsl.2012.06.041.

Danišík, M., Schmitt, A.K., Stockli, D.F., Lovera, O.M., Dunkl, I., Evans, N.J., 2017. Application of combined U-Th-disequilibrium/U-Pb and (U-Th)/He zircon dating to tephrochronology. Quat. Geochronol. 40, 23–32. https://doi.org/10.1016/j.quageo.2016.07.005.

Farley, K.A., 2002. (U-Th)/He dating: techniques, calibrations, and applications. Rev. Mineral. Geochem. 47 (1), 819–844. https://doi.org/10.2138/rmg.2002.47.18.

Farley, K.A., Kohn, B.P., Pillans, B., 2002. The effects of secular disequilibrium on (U–Th)/He systematics and dating of Quaternary volcanic zircon and apatite. Earth Planet. Sci. Lett. 201 (1), 117–125. https://doi.org/10.1016/S0012-821X(02)00659-3.

Fillerup, M.A., Knapp, J.H., Knapp, C.C., Raileanu, V., 2010. Mantle earthquakes in the absence of subduction? Continental delamination in the Romanian Carpathians. Lithosphere 2 (5), 333–340. https://doi.org/10.1130/L102.1.

Fisher, R.V., Schmincke, H.-U., 1984. Pyroclastic Rocks. Springer-Verlag, Berlin Heidelberg 978-3-642-74864-6 (472 pp).

Francalanci, L., Lucchi, F., Keller, J., De Astis, G., Tranne, C.A., 2013. Eruptive, volcano-tectonic and magmatic history of the Stromboli volcano (north-eastern Aeolian archipelago). In: Lucchi, F., Peccerillo, A., Keller, J., Tranne, C.A., Rossi, P.L. (Eds.), The Aeolian Islands Volcanoes. Geological Society, London, Memoirs. 37, pp. 397–471. https://doi.org/10.1144/M37.13.

Freda, C., Gaeta, M., Karner, D.B., Marra, F., Renne, P.R., Taddeucci, J., Scarlato, P., Christensen, J.N., Dallai, L., 2006. Eruptive history and petrologic evolution of the Albano multiple maar (Alban Hills, Central Italy). Bull. Volcanol. 68 (6), 567–591. https://doi.org/10.1007/s00445-005-0033-6.

Frey, H.M., Lange, R.A., Hall, C.M., Delgado-Granados, H., 2004. Magma eruption rates constrained by $^{40}Ar/^{39}Ar$ chronology and GIS for the Ceboruco–San Pedro volcanic field, western Mexico. GSA Bull. 116 (3–4), 259–276. https://doi.org/10.1130/B25321.1.

Frey, H.M., Lange, R.A., Hall, C.M., Nelson, S.A., Delgado-Granados, H., Mastin, L., Wineberg, D., 2014. $^{40}Ar/^{39}Ar$ geochronology of Volcán Tepetiltic, western Mexico: implications for the origin of zoned rhyodacite-rhyolite liquid erupted explosively from an andesite stratovolcano after a prolonged hiatus. GSA Bull. 126 (1–2), 16–30. https://doi.org/10.1130/B30790.1.

Gamble, J.A., Price, R.C., Smith, I.E.M., McIntosh, W.C., Dunbar, N.W., 2003. $^{40}Ar/^{39}Ar$ geochronology of magmatic activity, magma flux and hazards at Ruapehu volcano, Taupo Volcanic Zone, New Zealand. J. Volcanol. Geotherm. Res. 120 (1–4), 271–287. https://doi.org/10.1016/S0377-0273(02)00407-9.

Ghalamghash, J., Mousavi, S.Z., Hassanzadeh, J., Schmitt, A.K., 2016. Geology, zircon geochronology, and petrogenesis of Sabalan volcano (northwestern Iran). J. Volcanol. Geotherm. Res. 327, 192–207. https://doi.org/10.1016/j.jvolgeores.2016.05.001.

Gîrbacea, R., Frisch, W., 1998. Slab in the wrong place: lower lithospheric mantle delamination in the last stage of Eastern Carpathians subduction retreat. Geology 26, 611–614. https://doi.org/10.1130/0091-7613(1998)026<0611:SITWPL>2.3.CO;2.

Gropelli, G., Viereck-Goette, L., 2010. Stratigraphy and geology of volcanic areas. The Geological Society of America Special Paper https://doi.org/10.1007/s00445-013-0725-2 (464 p).

Halloul, N., Gourgaud, A., 2012. The post-collisional volcanism of northern Tunisia: petrology and evolution through time. J. Afr. Earth Sci. 63, 62–76. https://doi.org/10.1016/j.jafrearsci.2011.10.004.

Harangi, S., 2001. Neogene to Quaternary volcanism of the Carpathian–Pannonian Region — a review. Acta Geol. Hung. 44, 223–258.

Harangi, S., Lenkey, L., 2007. Genesis of the Neogene to Quaternary volcanism in the Carpathian-Pannonian region: role of subduction, extension, and mantle plume. In: Beccaluva, L., Bianchini, G., Wilson, M. (Eds.), Cenozoic Volcanism in the Mediterranean Area. Geological Society of America Special Paper, pp. 67–92 https://doi.org/10.1130/2007.2418(04).

Harangi, S., Molnár, M., Vinkler, A.P., Kiss, B., Jull, A.J.T., Leonard, A.G., 2010. Radiocarbon dating of the last volcanic eruptions of Ciomadul volcano, Southeast Carpathians, Eastern-Central Europe. Radiocarbon 52 (2–3), 1498–1507. https://doi.org/10.1017/S0033822200046580.

Harangi, S., Lukács, R., Schmitt, A.K., Dunkl, I., Molnár, K., Kiss, B., Seghedi, I., Novothny, Á., Molnár, M., 2015a. Constraints on the timing of Quaternary volcanism and duration of magma residence at Ciomadul volcano, east–central Europe, from combined U–Th/He and U–Th zircon geochronology. J. Volcanol. Geotherm. Res. 301, 66–80. https://doi.org/10.1016/j.jvolgeores.2015.05.002.

Harangi, S., Novák, A., Kiss, B., Seghedi, I., Lukács, R., Szarka, L., Wesztergom, V., Metwaly, M., Gribovszki, K., 2015b. Combined magnetotelluric and petrologic constrains for the nature of the magma storage system beneath the Late Pleistocene Ciomadul volcano (SE Carpathians). J. Volcanol. Geotherm. Res. 290, 82–96. https://doi.org/10.1016/j.jvolgeores.2014.12.006.

Harangi, Sz., Molnár, K., Kiss, B., Lukács, R., Dunkl, I., Schmitt, A.K., Seghedi, I., Novothny, Á., Molnár, M., Oross, R., Ntaflos, T., Mason, P.R.D., 2018. Eruption ages and geochemical fingerprints of the distal tephras from the Late Pleistocene Ciomadul Volcano, East Carpathians. INTAV-RO crossing new frontiers, INTAV International Field Conference on Tephrochronology "Tephra Hunt in Transylvania". In: Hambach, Ulrich, Veres, Daniel (Eds.), Book of Abstracts, pp. 53–54.

Hildreth, W., Lanphere, M.A., 1994. Potassium–argon geochronology of a basalt–andesite–dacite arc system: the Mt. Adams volcanic field, Cascade Range of southern Washington. Geol. Soc. Am. Bull. 106, 1413–1429. https://doi.org/10.1130/0016-7606(1994)106<1413:PAGOAB>2.3.CO;2.

Hora, J.M., Singer, B.S., Wörner, G., 2007. Volcano evolution and eruptive flux on the thick crust of the Andean Central Volcanic Zone: 40Ar/39Ar constraints from Volcán Parinacota, Chile. Geol. Soc. Am. Bull. 119 (3–4), 343–362. https://doi.org/10.1130/B25954.1.

Hoshizumi, H., Uto, K., Watanabe, K., 1999. Geology and eruptive history of Unzen volcano, Shimabara Peninsula, Kyushu, SW Japan. J. Volcanol. Geotherm. Res. 89 (1–4), 81–94. https://doi.org/10.1016/S0377-0273(98)00125-5.

Hourigan, J.K., Reiners, P.W., Brandon, M.T., 2005. U-Th zonation-dependent alpha-ejection in (U-Th)/He chronometry. Geochim. Cosmochim. Acta 69 (13), 3349–3365. https://doi.org/10.1016/j.gca.2005.01.024.

Karátson, D., 2007. A Börzsönytől a Hargitáig — vulkanológia, felszínfejlődés, ősföldrajz. Typotex Kiadó, Budapest (463 pp).

Karátson, D., Tímár, G., 2005. Comparative volumetric calculations of two segments of the Neogene/Quaternary volcanic chain using SRTM elevation data: implications for erosion and magma output rates. Z. Geomorphol. Suppl. 140, 19–35.

Karátson, D., Telbisz, T., Harangi, S., Magyari, E., Dunkl, I., Kiss, B., Jánosi, C., Veres, D., Braun, M., Fodor, E., Biró, T., Kósik, S., von Eynatten, H., Lin, D., 2013. Morphometrical and geochronological constraints on the youngest eruptive activity in East-Central Europe at the Ciomadul (Csomád) lava dome complex, East Carpathians. J. Volcanol. Geotherm. Res. 255 (0), 43–56. https://doi.org/10.1016/j.jvolgeores.2013.01.013.

Karátson, D., Wulf, S., Veres, D., Magyari, E.K., Gertisser, R., Timar-Gabor, A., Novothny, Á., Telbisz, T., Szalai, Z., Anechitei-Deacu, V., Appelt, O., Bormann, M., Jánosi, C., Hubay, K., Schäbitz, F., 2016. The latest explosive eruptions of Ciomadul (Csomád) volcano, East Carpathians — a tephrostratigraphic approach for the 51–29 ka BP time interval. J. Volcanol. Geotherm. Res. 319, 29–51. https://doi.org/10.1016/j.jvolgeores.2016.03.005.

Kasapoğlu, B., Ersoy, Y.E., Uysal, İ., Palmer, M.R., Zack, T., Koralay, E.O., Karlsson, A., 2016. The petrology of Paleogene volcanism in the Central Sakarya, Nallıhan Region: Implications for the initiation and evolution of post-collisional, slab break-off-related magmatic activity. Lithos 246-247, 81–98. https://doi.org/10.1016/j.lithos.2015.12.024.

Kiss, B., Harangi, S., Ntaflos, T., Mason, P.R.D., Pál-Molnár, E., 2014. Amphibole perspective to unravel pre-eruptive processes and conditions in volcanic plumbing systems beneath intermediate arc volcanoes: a case study from Ciomadul volcano (SE Carpathians). Contrib. Mineral. Petrol. 167 (3), 1–27. https://doi.org/10.1007/s00410-014-0986-6.

Klemetti, E.W., Clynne, M.A., 2014. Localized Rejuvenation of a Crystal Mush Recorded in Zircon Temporal and Compositional Variation at the Lassen Volcanic Center, Northern California. PLoS ONE 9 (12), e113157. https://doi.org/10.1371/journal.pone.0113157.

Klemetti, E.W., Grunder, A.L., 2008. Volcanic evolution of Volcán Aucanquilcha: a long-lived dacite volcano in the Central Andes of northern Chile. Bull. Volcanol. 70, 633–650. https://doi.org/10.1007/s00445-007-0158-x.

Konečný, V., Kovác, M., Lexa, J., Šefara, J., 2002. Neogene evolution of the Carpatho-Pannonian region: an interplay of subduction and back-arc diapiric uprise in the mantle. European Geophysical Union Stephan Mueller Special Publication Series vol. 1, pp. 105–123.

Lewis-Kenedi, C.B., Lange, R.A., Hall, C.M., Delgado-Granados, H., 2005. The eruptive history of the Tequila volcanic field, western Mexico: ages, volumes, and relative proportions of lava types. Bull. Volcanol. 67, 391–414. https://doi.org/10.1007/s00445-004-0377-3.

Lexa, J., Seghedi, I., Németh, K., Szakács, A., Konecny, V., Pécskay, Z., Fülöp, A., Kovacs, M., 2010. Neogene-Quaternary Volcanic forms in the Carpathian-Pannonian Region: a review. Cent. Eur. J. Geosci. 2 (3), 207–270. https://doi.org/10.2478/v10085-010-0024-5.

Lucchi, F., 2013. Stratigraphic methodology for the geological mapping of volcanic areas: insights from the Aeolian archipelago (southern Italy). In: Lucchi, F., Peccerillo, A., Keller, J., Tranne, C.A., Rossi, P.L. (Eds.), The Aeolian Islands Volcanoes. Geological Society, London, Memoirs 37, pp. 37–53. https://doi.org/10.1144/M37.5.

Lukács, R., Harangi, Sz, Guillong, M., Bachmann, O., Fodor, L., Buret, Y., Dunkl, I., Sliwinski, J., von Quadt, A., Peytcheva, I., Zimmerer, M., 2018a. Early to Mid-Miocene syn-extensional massive silicic volcanism in the Pannonian Basin (East-Central Europe): eruption chronology, correlation potential and geodynamic implications. Earth Sci. Rev. 179, 1–19. https://doi.org/10.1016/j.earscirev.2018.02.005.

Lukács, R., Guillong, M., Schmitt, A.K., Molnár, K., Harangi, Sz, Bachmann, O., 2018b. LA-ICP-MS and SIMS U-Pb and U-Th zircon geochronology of Late Pleistocene lava domes of the Ciomadul Volcanic Dome Complex (Eastern Carpathians). Data Brief 18, 808–813. https://doi.org/10.1016/j.dib.2018.03.100.

Lukács, R., Schmitt, A.K., Caricchi, L., Bachmann, O., Guillong, M., Molnár, K., Harangi, Sz, 2019. Long-living crystal mush system beneath the Ciomadul volcanic dome field (Eastern-Central Europe) based on zircon crystallization age distribution. EGU Gen. Assem. 2019, EGU2019–15118.

Martin, M., Wenzel, F., Calixto, W.G., 2006. High-resolution teleseismic body wave tomography beneath SE-Romania – II. Imaging of a slab detachment scenario. Geophys. J. Int. 164 (3), 579–595. https://doi.org/10.1111/j.1365-246X.2006.02884.x.

Mason, P.R.D., Downes, H., Thirlwall, M., Seghedi, I., Szakács, A., Lowry, D., Mattey, D., 1996. Crustal assimilation as a major petrogenetic process in east Carpathian Neogene to Quaternary continental margin arc magmas. J. Petrol. 37, 927–959.
Mason, P.R.D., Seghedi, I., Szakács, A., Downes, H., 1998. Magmatic constraints on geodynamic models of subduction in the East Carpathians, Romania. Tectonophysics 297, 157–176. https://doi.org/10.1016/S0040-1951(98)00167-X.
Molnár, K., 2014. A Csomád vulkáni komplexum geokronológiai vizsgálata (U-Th)/He-módszerrel (DK-i Kárpátok). Eötvös Loránd University, Budapest (97 pp).
Molnár, K., Harangi, S., Lukács, R., Dunkl, I., Schmitt, A.K., Kiss, B., Garamhegyi, T., Seghedi, I., 2018. The onset of the volcanism in the Ciomadul Volcanic Dome Complex (Eastern Carpathians): eruption chronology and magma type variation. J. Volcanol. Geotherm. Res. 354, 39–56. https://doi.org/10.1016/j.jvolgeores.2018.01.025.
Moriya, I., Okuno, M., Nakamura, E., Szakács, A., Seghedi, I., 1995. Last Eruption and Its 14C Age of Ciomadul Volcano, Romania. Summaries of Researches Using AMS at Nagoya University. 6 pp. 82–91.
Moriya, I., Okuno, M., Nakamura, E., Szakács, A., Seghedi, I., 1996. Radiocarbon Ages of Charcoal Fragments From the Pumice Flow Deposits of the Last Eruption of Ciomadul Volcano, Romania. Summaries of Researches Using AMS at Nagoya University (VII). 3 pp. 252–255.
Nakamura, N., 1974. Determination of REE, Ba, Fe, Mg, Na and K in carbonaceous and ordinary chondrites. Geochim. Cosmochim. Acta 38 (5), 757–775. https://doi.org/10.1016/0016-7037(74)90149-5.
Oncescu, M.C., Burlacu, V., Anghel, M., Smalbergher, V., 1984. Three-dimensional P-wave velocity image under the Carpathian arc. Tectonophysics 106 (3), 305–319.
Paces, J.B., Miller Jr., J.D., 1993. Precise U-Pb ages of Duluth Complex and related mafic intrusions, northeastern Minnesota: geochronological insights to physical, petrogenetic, paleomagnetic, and tectonomagnetic processes associated with the 1.1 Ga Midcontinent Rift System. J. Geophys. Res. 98 (8), 13997–14013.
Panaiotu, C.G., Jicha, B.R., Singer, B.S., Ţugui, A., Seghedi, I., Panaiotu, A.G., Necula, C., 2013. $^{40}Ar/^{39}Ar$ chronology and paleomagnetism of Quaternary basaltic lavas from the Perşani Mountains (East Carpathians). Phys. Earth Planet. Inter. 221, 1–14. https://doi.org/10.1016/j.pepi.2013.06.007.
Peccerillo, A., Taylor, S.R., 1976. Geochemistry of eocene calc-alkaline volcanic rocks from the Kastamonu area, Northern Turkey. Contrib. Mineral. Petrol. 58 (1), 63–81.
Pécskay, Z., Lexa, J., Szkécs, A., Balogh, K., Seghedi, I., Konecny, V., Kovács, M., Márton, E., Kaliciak, M., Széky-Fux, V., Póka, T., Gyarmati, P., Edelstein, O., Rosu, E., Zec, B., 1995. Space and time distribution of Neogene-Quaternary volcanism in the Carpatho-Pannonian Region. In: Downes, H., Vaselli, O. (Eds.), Neogene and Related Magmatism in the Carpatho-Pannonian Region. Acta Vulcanologica, pp. 15–28.
Pécskay, Z., Lexa, J., Szakács, A., Seghedi, I., Balogh, K., Konecný, V., Zelenka, T., Kovacs, M., Póka, T., Fülöp, A., Márton, E., Panaiotu, C., Cvetkovic, V., 2006. Geochronology of Neogene magmatism in the Carpathian arc and intra-Carpathian area. Geol. Carpath. 57 (6), 511–530.
Popa, M., Radulian, M., Szakács, A., Seghedi, I., Zaharia, B., 2012. New seismic and tomography data in the southern part of the Harghita Mountains (Romania, Southeastern Carpathians): connection with recent volcanic activity. Pure Appl. Geophys. 169 (9), 1557–1573. https://doi.org/10.1007/s00024-011-0428-6.
Reiners, P.W., 2005. Zircon (U-Th)/He thermochronometry. Rev. Mineral. Geochem. 58 (1), 151–179.
Samaniego, P., Barba, D., Robin, C., Fornari, M., Bernard, B., 2012. Eruptive history of Chimborazo volcano (Ecuador): a large, ice-capped and hazardous compound volcano in the Northern Andes. J. Volcanol. Geotherm. Res. 221–222, 33–51. https://doi.org/10.1016/j.jvolgeores.2012.01.014.
Schmitt, A.K., 2011. Uranium series accessory crystal dating of magmatic processes. Annu. Rev. Earth Planet. Sci. 39 (1), 321–349. https://doi.org/10.1146/annurev-earth-040610-133330.
Schmitt, A.K., Stockli, D.F., Hausback, B.P., 2006. Eruption and magma crystallization ages of Las Tres Vírgenes (Baja California) constrained by combined $^{230}Th/^{238}U$ and (U–Th)/He dating of zircon. J. Volcanol. Geotherm. Res. 158 (3–4), 281–295. https://doi.org/10.1016/j.jvolgeores.2006.07.005.
Schmitt, A.K., Stockli, D.F., Niedermann, S., Lovera, O.M., Hausback, B.P., 2010. Eruption ages of Las Tres Vírgenes volcano (Baja California): a tale of two helium isotopes. Quat. Geochronol. 5 (5), 503–511. https://doi.org/10.1016/j.quageo.2010.02.004.
Schmitt, A.K., Danišík, M., Aydar, E., Şen, E., Ulusoy, I., Lovera, O.M., 2014. Identifying the volcanic eruption depicted in a Neolithic Painting at Çatalhöyük, Central Anatolia, Turkey. PLoS ONE 9 (1), e84711. https://doi.org/10.1371/journal.pone.0084711.
Schmitt, A.K., Konrad, K., Andrews, G.D.M., Horie, K., Brown, S.R., Koppers, A.A.P., Pecha, M., Busby, C.J., Tamura, Y., 2017. $^{40}Ar/^{39}Ar$ ages and zircon petrochronology for the rear arc of the Izu-Bonin-Marianas intra-oceanic subduction zone. Int. Geol. Rev. 60 (8), 956–976. https://doi.org/10.1080/00206814.2017.1363675.
Seghedi, I., Downes, H., 2011. Geochemistry and tectonic development of Cenozoic magmatism in the Carpathian–Pannonian region. Gondwana Res. 20 (4), 655–672. https://doi.org/10.1016/j.gr.2011.06.009.
Seghedi, I., Szakács, A., Udrescu, C., Stoian, M., Grabari, G., 1987. Trace element geochemistry of the South Hargitha volcanics (East Carpathians): calc-alkaline and shoshonitic association. Dari de Seama ale Sedintelor Institutul de Geologie si Geofizica. 72–73, pp. 381–397.
Seghedi, I., Szakács, A., Mason, P.R.D., 1995. Petrogenesis and magmatic evolutions in the East Carpathians Neogene volcanic arc (Romania). Acta Vulcanol. 7, 135–145.
Seghedi, I., Balintoni, I., Szakács, A., 1998. Interplay of tectonics and neogene post-collisional magmatism in the Intracarpathian region. Lithos 45 (1–4), 483–497. https://doi.org/10.1016/S0024-4937(98)00046-2.
Seghedi, I., Downes, H., Szakács, A., Mason, P.R.D., Thirlwall, M.F., Rosu, E., Pécskay, Z., Marton, E., Panaiotu, C., 2004. Neogene-Quaternary magmatism and geodynamics in the Carpathian-Pannonian region: a synthesis. Lithos 72, 117–146. https://doi.org/10.1016/j.lithos.2003.08.006.
Seghedi, I., Downes, H., Harangi, Sz, Mason, P.R.D., Pécskay, Z., 2005. Geochemical response of magmas to Neogene-Quaternary continental collision in the Carpathian-Pannonian region: a review. Tectonophysics 410 (1–4), 485–499. https://doi.org/10.1016/j.tecto.2004.09.015.
Seghedi, I., Maţenco, L., Downes, H., Mason, P.R.D., Szakács, A., Pécskay, Z., 2011. Tectonic significance of changes in post-subduction Pliocene–Quaternary magmatism in the south east part of the Carpathian–Pannonian Region. Tectonophysics 502 (1–2), 146–157. https://doi.org/10.1016/j.tecto.2009.12.003.
Siebert, L., Simkin, T., Kimberly, P., 2011. Volcanoes of the World. University of California Press (568 pp).
Singer, B.S., Thompson, R.A., Dungan, M.A., Feeley, T.C., Nelson, S.T., Pickens, J.C., Brown, L.L., Wulff, A.W., Davison, J.P., Metzger, J., 1997. Volcanism and erosion during the past 930 k.y. at the Tatara-San Pedro complex, Chilean Andes. GSA Bull. 109 (2), 127–142. https://doi.org/10.1130/0016-7606(1997)109<0127:VAEDTP>2.3.CO;2.
Sperner, B., Lorenz, F., Bonjer, K., Hettel, S., Muller, B., Wenzel, F., 2001. Slab break-off - abrupt cut or gradual detachment? New insights from the Vrancea Region (SE Carpathians, Romania). Terra Nova 13, 172–179. https://doi.org/10.1046/j.1365-3121.2001.00335.x.
Szabó, C., Harangi, S., Csontos, L., 1992. Review of neogene and quaternary volcanism of the Carpathian-Pannonian region: a review. Tectonophysics 208, 243–256. https://doi.org/10.1016/0040-1951(92)90347-9.
Szakács, A., Seghedi, I., 1995. The Călimani-Gurghiu-Harghita volcanic chain, East Carpathians, Romania: volcanological features. Acta Vulcanol. 7 (2), 145–153.
Szakács, A., Seghedi, I., Pécskay, Z., 1993. Peculiarities of South Harghita Mts. as the terminal segment of the Carpathian Neogene to Quaternary volcanic chain. Rev. Roum. Géol. Géophys. Géog. Géol. 37, 21–37.
Szakács, A., Seghedi, I., Pécskay, Z., Mirea, V., 2015. Eruptive history of a low-frequency and low-output rate Pleistocene volcano, Ciomadul, South Harghita Mts., Romania. Bull. Volcanol. 77 (2), 1–19. https://doi.org/10.1007/s00445-014-0894-7.
Trasatti, E., Marra, F., Polcari, M., Etiope, G., Ciotoli, G., Darrah, T.H., Tedesco, D., Stramondo, S., Florindo, F., Ventura, G., 2018. Coeval uplift and subsidence reveal magma recharging near Rome (Italy). Geochem. Geophys. Geosyst. 19 (5), 1484–1498. https://doi.org/10.1029/2017GC007303.
Vinkler, A.P., Harangi, S., Ntaflos, T., Szakács, A., 2007. A Csomád vulkán (Keleti-Kárpátok) horzsaköveinek kőzettani és geokémiai vizsgálata - petrogenetikai következtetések. Földtani Közlöny 137 (1), 103–128.
Wiedenbeck, M., Hanchar, J.M., Peck, W.H., Sylvester, P., Valley, J., Whitehouse, M., Kronz, A., Morishita, Y., Nasdala, L., Fiebig, J., Franchi, I., Girard, J.P., Greenwood, R.C., Hinton, R., Kita, N., Mason, P.R.D., Norman, M., Ogasawara, M., Piccoli, P.M., Rhede, D., Satoh, H., Schulz-Dobrick, B., Skår, O., Spicuzza, M.J., Terada, K., Tindle, A., Togashi, S., Vennemann, T., Xie, Q., Zheng, Y.F., 2004. Further characterisation of the 91500 zircon crystal. Geostand. Geoanal. Res. 28 (1), 9–39. https://doi.org/10.1111/j.1751-908X.2004.tb01041.x.
Wörner, G., Hammerschmidt, K., Henjes-Kunst, F., Lezaun, J., Wilke, H., 2000. Geochronology ($^{40}Ar/^{39}Ar$, K-Ar and He-exposure ages) of Cenozoic magmatic rocks from Northern Chile (18–22°S): implications for magmatism and tectonic evolution of the central Andes. Rev. Geol. Chile 27 (2), 205–240. https://doi.org/10.4067/S0716-02082000000200004.